AD-A131 174 ASYMMETRIC COLLAPSE OF LOS PIPE-LS-4(U) PHYSICS 1/1
INTERNATIONAL CO SAN LEANDRO CA D MUMMA ET AL.
01 MAR 82 PIFR-1403 DNA-6141F DNA001-80-C-0108

UNCLASSIFIED F/G 18/3 NL

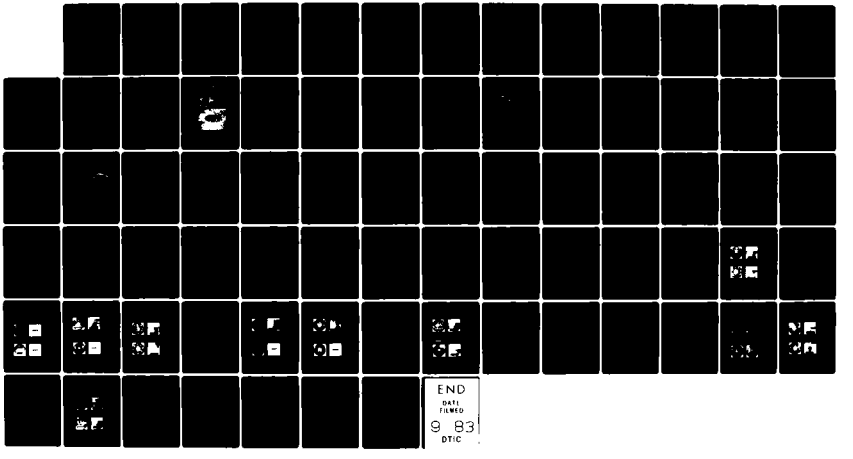

END
DATE FILMED
9 83
DTIC

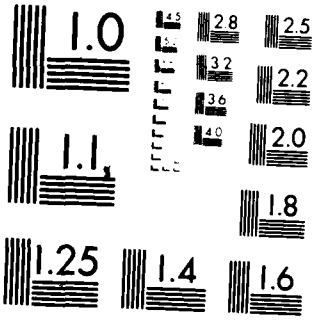

(12)

DNA 6141F

ASYMMETRIC COLLAPSE OF LOS PIPE—LS-4

Physics International Company
2700 Merced Street
San Leandro, California 94577

1 March 1982

Final Report for Period 1 February 1980—1 December 1980

CONTRACT No. DNA 001-80-C-0108

APPROVED FOR PUBLIC RELEASE;
DISTRIBUTION UNLIMITED.

THIS WORK WAS SPONSORED BY THE DEFENSE NUCLEAR AGENCY
UNDER RDT&E RMSS CODE B345080462 J24AAXYX98375 H2590D.

Prepared for
Director
DEFENSE NUCLEAR AGENCY
Washington, DC 20305

UNCLASSIFIED

SECURITY CLASSIFICATION OF THIS PAGE (When Data Entered)

REPORT DOCUMENTATION PAGE	READ INSTRUCTIONS BEFORE COMPLETING FORM
1. REPORT NUMBER: DNA 6141F	2. GOVT ACCESSION NO.: AD A131174	3. RECIPIENT'S CATALOG NUMBER:
4. TITLE (and Subtitle): ASYMMETRIC COLLAPSE OF LOS PIPE—LS-4	5. TYPE OF REPORT & PERIOD COVERED: Final Report for Period 1 Feb 80—1 Dec 80
	6. PERFORMING ORG. REPORT NUMBER: PIFR-1403
7. AUTHOR(s): D. Mumma, J. Thomsen, R. Funston, and E. T. Moore, Jr.	8. CONTRACT OR GRANT NUMBER(s): DNA 001-80-C-0108
9. PERFORMING ORGANIZATION NAME AND ADDRESS: Physics International Company, 2700 Merced Street, San Leandro, California 94577	10. PROGRAM ELEMENT, PROJECT, TASK AREA & WORK UNIT NUMBERS: Subtask J24AAXYX983-75
11. CONTROLLING OFFICE NAME AND ADDRESS: Director, Defense Nuclear Agency, Washington, D.C. 20305	12. REPORT DATE: 1 March 1982
	13. NUMBER OF PAGES: 76
14. MONITORING AGENCY NAME & ADDRESS(if different from Controlling Office)	15. SECURITY CLASS. (of this report): UNCLASSIFIED
	15a. DECLASSIFICATION/DOWNGRADING SCHEDULE: N/A since UNCLASSIFIED

16. DISTRIBUTION STATEMENT (of this Report)

Approved for public release; distribution unlimited.

17. DISTRIBUTION STATEMENT (of the abstract entered in Block 20, if different from Report)

18. SUPPLEMENTARY NOTES

This work was sponsored by the Defense Nuclear Agency under RDT&E RMSS Code B345080462 J24AAXYX98375 H2590D.

19. KEY WORDS (Continue on reverse side if necessary and identify by block number)

LOS Flow Simulation
Particulate Jetting

20. ABSTRACT (Continue on reverse side if necessary and identify by block number)

This report summarizes the results of a single laboratory experiment (LS-4) that was performed to further evaluate the feasibility of using asymmetries to suppress jetting in line-of-sight (LOS) pipes collapsed by the ground shock from an underground nuclear test. Underground conditions were simulated by using a sphere of high explosive to collapse twenty-six small-scale models embedded in saturated sand.

(continued)

DD FORM 1 JAN 73 1473 EDITION OF 1 NOV 65 IS OBSOLETE

UNCLASSIFIED

SECURITY CLASSIFICATION OF THIS PAGE (When Data Entered)

20. ABSTRACT (continued)

Thin-walled, straight, stainless steel tubes were used to model LOS pipes. Models with no further alterations were called "standard" models. Other models contained some form of asymmetry added to the tube to alter the pipe collapse and jet formation process or to attenuate the jet after it is formed.

The results of the experiment show that high-energy jetting of standard models always occurs, is enhanced by increasing the areal density of the pipe wall, and is unaffected by the presence of air in the pipe. Jet energy decreases with the pipe standoff relative to the surface of the high explosive sphere. The use of helical or ring asymmetries was effective in attenuating the jet in all cases where the asymmetry was loosely attached to the inner wall of the pipe, even when it was positioned beyond the jet forming region of the pipe. Very little jet attenuation was observed when a ring or helical asymmetry was located entirely within an expansion chamber.

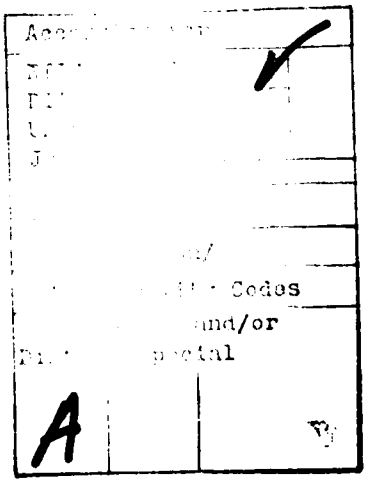

CONVERSION FACTORS FOR U.S. CUSTOMARY TO METRIC (SI) UNITS OF MEASUREMENT

To Convert From	To	Multiply By
angstrom	meters (m)	1.000 000 X E -10
atmosphere (normal)	kilo pascal (kPa)	1.013 25 X E +2
bar	kilo pascal (kPa)	1.000 000 X E +2
British thermal unit (thermochemical)	joule (J)	1.054 350 X E +3
cal (thermochemical)/cm^2 ‡	mega joule/m^2	4.184 000 X E-2
calorie (thermochemical) ‡	joule (J)	4.184 000
calorie (thermochemical)/g‡	joule per kilogram (J/kg)*	4.184 000 X E +3
curie‡	giga becquerel (GBq)+	3.700 000 X E +1
degree Celsius#	degree kelvin (K)	$T_K = T°_C + 273.15$
degree (angle)	radian (rad)	1.745 329 X E -2
degree Fahrenheit	degree kelvin (K)	$T_K = (T°F + 459.67)/1.8$
electron volt‡	joule (J)	1.602 19 X E -19
erg‡	joule (J)	1.000 000 X E -7
erg/second	watt (W)	1.000 000 X E -7
foot	meter (m)	3.048 000 X E-1
foot-pound-force	joule (J)	1.355 818
gallon (U.S. liquid)	meter^3 (m^3)	3.785 412 X E -3
inch	meter (m)	2.540 000 X E -2
jerk	joule (J)	1.000 000 X E +9
joule/kilogram (J/kg) (radiation dose absorbed)‡	gray (Gy)*	1.000 000
kilotons‡	terajoules	4.183
kip (1000 lbf)	newton (N)	4.448 222 X E +3
kip/inch^2 (ksi)	kilo pascal (kPa)	6.894 757 X E +3
ktap	newton-second/m^2 (N-s/m^2)	1.000 000 X E +2
micron	meter (m)	1.000 000 X E -6
mil	meter (m)	2.540 000 X E -5
mile (international)	meter (m)	1.609 344 X E +3
ounce	kilogram (kg)	2.834 952 X E -2
pound-force (lbf avoirdupois)	newton (N)	4.448 222
pound-force inch	newton-meter (N-m)	1.129 848 X E -1
pound-force/inch	newton/meter (N/m)	1.751 268 X E +2
pound-force/foot^2	kilo pascal (kPa)	4.788 026 X E -2
pound-force/inch^2 (psi)	kilo pascal (kPa)	6.894 757
pound-mass (lbm avoirdupois)	kilogram (kg)	4.535 924 X E -1
pound-mass-foot^2 (moment of inertia)	kilogram-meter^2 (kg*m^2)	4.214 011 X E -2
pound-mass/foot^3	kilogram-meter^3)	1.601 846 X E +1
rad (radiation dose absorbed)‡	gray (Gy)*	1.000 000 X E -2
roentgen‡	coulomb/kilogram (C/kg)	2.579 760 X E -4
shake	second (s)	1.000 000 X E -8
slug	kilogram (kg)	1.459 390 X E +1
torr (mm Hg, 0° C)	kilo pascal (kPa)	1.333 22 X E -1

*The gray (Gy) is the accepted SI unit equivalent to the energy imparted by ionizing radiation to a mass of energy corresponding to one joule/kilogram.
+ The becquerel (Bq) is the SI unit of radioactivity; 1 Bq = 1 event/s.
# Temperature may be reported in degree Celsius as well as degree kelvin.
‡These units should not be converted in DNA technical reports; however, a parenthetical conversion is permitted at the author's discretion.

TABLE OF CONTENTS

LIST OF ILLUSTRATIONS

LIST OF ILLUSTRATIONS (Cont.)

LIST OF ILLUSTRATIONS (Cont.)

SECTION 1
INTRODUCTION

1.1 BACKGROUND

Line-of-sight (LOS) pipes are frequently used in underground nuclear tests (UGT) to collimate and transmit the radiation from a nuclear source to an experimental test station. The radiation is followed by a spherically divergent ground shock that causes the LOS pipe to collapse and form a high-energy jet. Occasionally, this jet constitutes a threat not only to the experimental objectives of the underground test, but also to the successful containment of the radioactive materials resulting from the test. The work reported here is part of the Defense Nuclear Agency's continuing effort to minimize the effects of jetting in LOS pipes and thereby optimize the safety and data retrieval associated with their underground nuclear weapon effects testing program.

This report summarizes the results of a single experiment designated (LS-4) that was performed in a continuing series to further investigate jetting phenomena in small-scale LOS models. This experiment represents the final task of a program that was structured to evaluate the feasibility of using asymmetries to either inhibit the formation of jets or to attenuate the severity of jets after they are formed. Results from previous experiments

(LS-1 through LS-3) showed that thin helical ribbons of polyolefin, steel, or lead placed on the inside surface of a straight LOS pipe model were an effective method of eliminating passive target damage caused by jetting (References 1 and 2). It was demonstrated in previous tests that a thick internal helical spiral placed at the far end of a standard LOS pipe appeared to be equally effective in preventing target damage.

1.2 OBJECTIVES

A major objective of the LS-4 experiment was to investigate the ability of the full-length thin internal helix to eliminate target damage from jetting in straight pipes for a variety of enhanced jetting conditions. Emphasis was also placed on determining how the helix operates by placing it only in various portions of the LOS pipe model. Did the helix operate by suppressing jet formation, or by attenuating the jetted flow once it was formed? Evidence from past experiments suggested that if a thick internal spiral were inserted at only the far end of an LOS pipe model, the jet flow would be attenuated. It was not known, however, if the thin (standard thickness) helix would be equally as effective.

A secondary objective was to investigate the effectiveness of expansion chambers and ring asymmetries in attenuating the jetted flow. Standard LOS pipe models were also included to increase the data base developed in previous experiments and as a controlled indicator of shot-to-shot repeatability.

SECTION 2

DESCRIPTION OF EXPERIMENT (LS-4)

2.1 CONCEPT

The LS-4 experiment was devised to simulate the conditions that exist during the collapse of an LOS pipe in an underground nuclear test. This experiment consisted of 26 small steel tubes positioned radially around a sphere containing liquid high explosive and embedded in saturated sand. The tubes, explosive, and sand were used to represent respectively the LOS pipes, the nuclear device, and the geological media in an underground nuclear test. The configuration of this experiment is shown schematically in Figure 1. A more complete description of the individual components of the experiment is given below.

2.2 EXPERIMENTAL APPARATUS

2.2.1 Explosive Source. The explosive source is shown in Figure 2. Approximately 136 kg of liquid nitromethane was contained in a 61.0-cm-diameter fiberglass sphere. This explosive has a detonation pressure of 14 GPa (140 kbar), comparable to the calculated peak free-field radial stress at a range of interest for a nuclear event such as MIGHTY EPIC.

A booster assembly was used to initiate detonation in the nitromethane at the center of the sphere. It was placed into

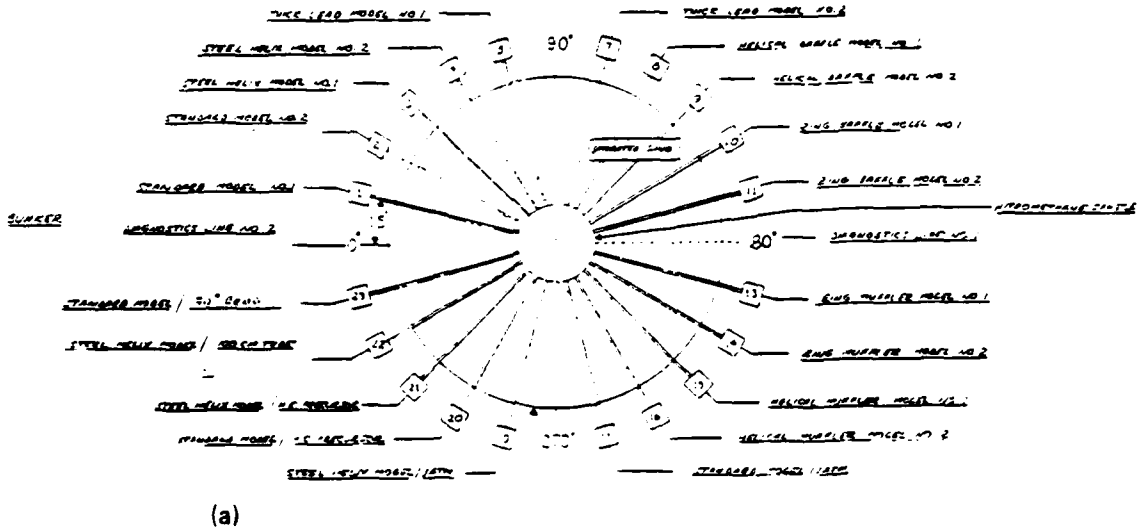

(a)

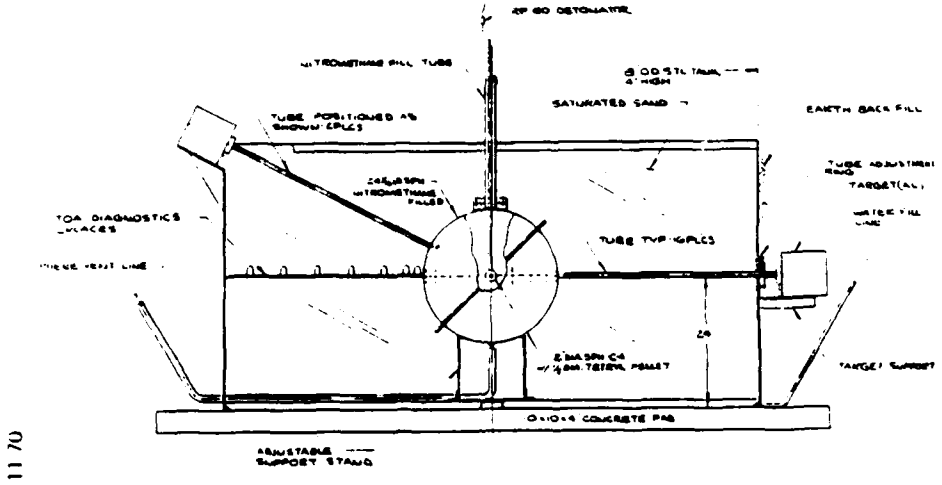

(b)

Figure 1 Spherical high explosive experiment for investigating the effects of asymmetries in LOS models: (a) plan view, and (b) cross section

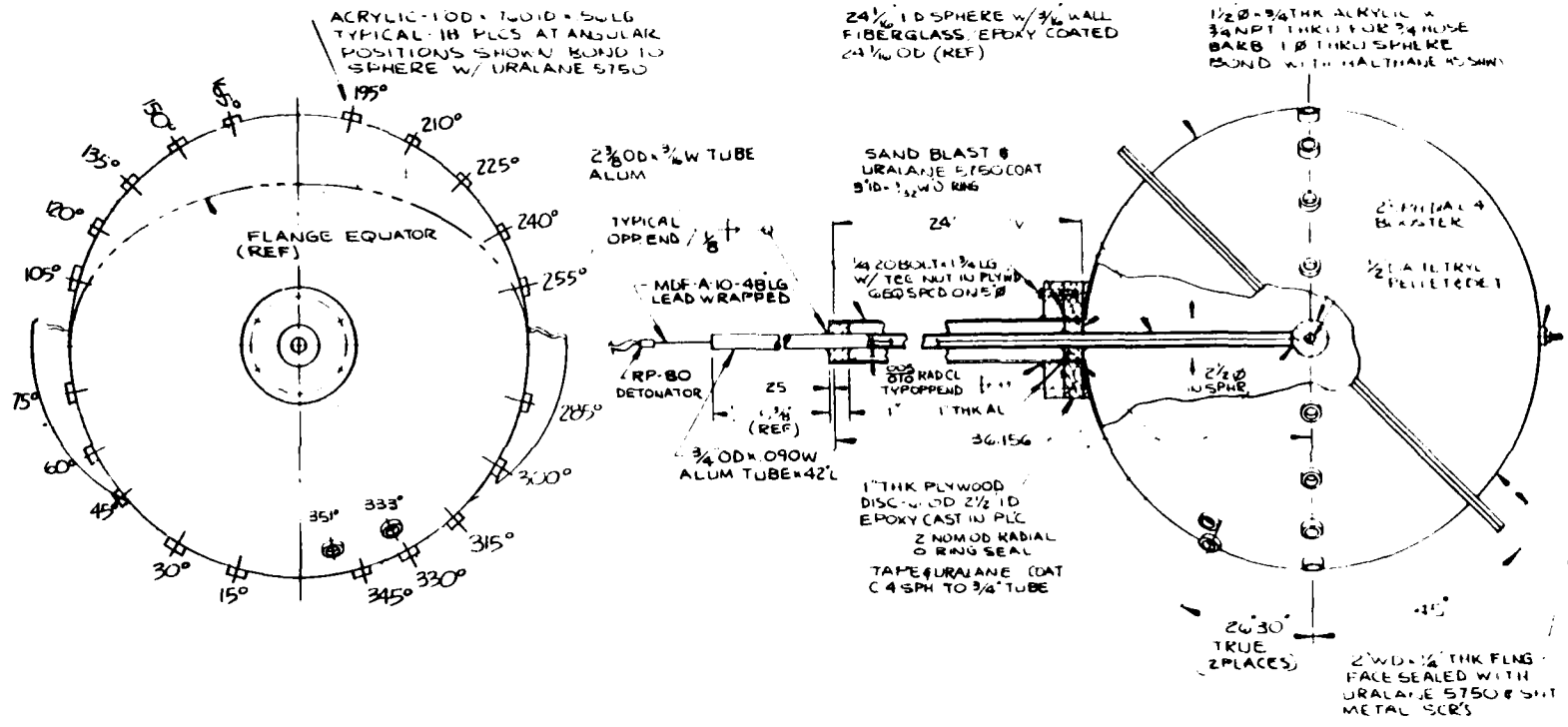

80-4-51

Figure 2. Explosive source used in LS-4.

position through a vertical fill tube at the top of the sphere. The booster assembly was an explosive train consisting of a 1.25-cm-diameter tetryl pellet and a length of mild detonating fuse (MDF) which extended beyond the top of the fill tube. The detonation sequence in the explosive train was initiated by an RP-80 exploding bridgewire detonator located at the end of the fuse.

2.2.2 LOS Models. The models were fabricated from 19-mm-diameter welded and drawn AISI type 321 stainless steel tubes (Military Specification T-8808). All of the tubes had a wall thickness of 0.305 mm. After the tubes were cut to the desired length, a steel plug was bonded onto the end of the tube facing the explosive sphere. An aluminum flange was bonded onto the opposite end of each tube. This flange was used to support a thin Mylar diaphragm and a vacuum port. Aluminum targets were then placed against the flange of each model. Two models contained one atmosphere of air while the remaining LOS models were evacuated to a pressure less than 1.0 mm Hg.

As shown in Figure 1, the models were designated either by title or by a model number, which was also its position around the explosive sphere. Twenty LOS models were located in the horizontal midplane of the sphere. The six remaining models were elevated above the midplane, as illustrated in the cross-sectional view of Figure 1. All models were inserted into precisely located Lucite positioning rings on the surface of the explosive sphere and carefully aligned perpendicular to this surface.

2.2.3 Test Bed. The saturated sand test bed was contained in a cylindrical steel tank. The tank was formed by rolling and welding a 6.4-mm-thick steel plate into a 2.44-m-diameter steel cylinder and reinforcing the top and bottom of the tank with U-channel. The tank was then placed on a concrete pad. The LOS models and instrumentation lines were positioned radially from the explosive sphere, which was located at the center of the tank. A photograph of these items appears in Figure 3a.

The test bed was prepared by carefully pouring sacks of Monterey sand into water which was controlled by a water distribution system around the perimeter of the bottom of the tank. The water distribution system consisted of perforated plastic tubing contained in a bed of pea-sized gravel. Care was taken to maintain a thin slurry of sand and water in the tank at all times. The slurry was mixed by hand to assure thorough wetting of the sand grains and to avoid trapping air bubbles. Figure 3b is a photograph of the experimental setup after the tank has been filled with sand.

The instrumentation for determining the time-of-arrival (TOA) of the shock wave in the saturated sand was located at positions 0° and 180° (Figure 2). In a similar manner, the horizontal plane of positions 90° and 180° contained the flange joint for the two fiberglass hemispheres that formed the explosive sphere. The flange was oriented at a 45° angle with respect to the horizontal plane.

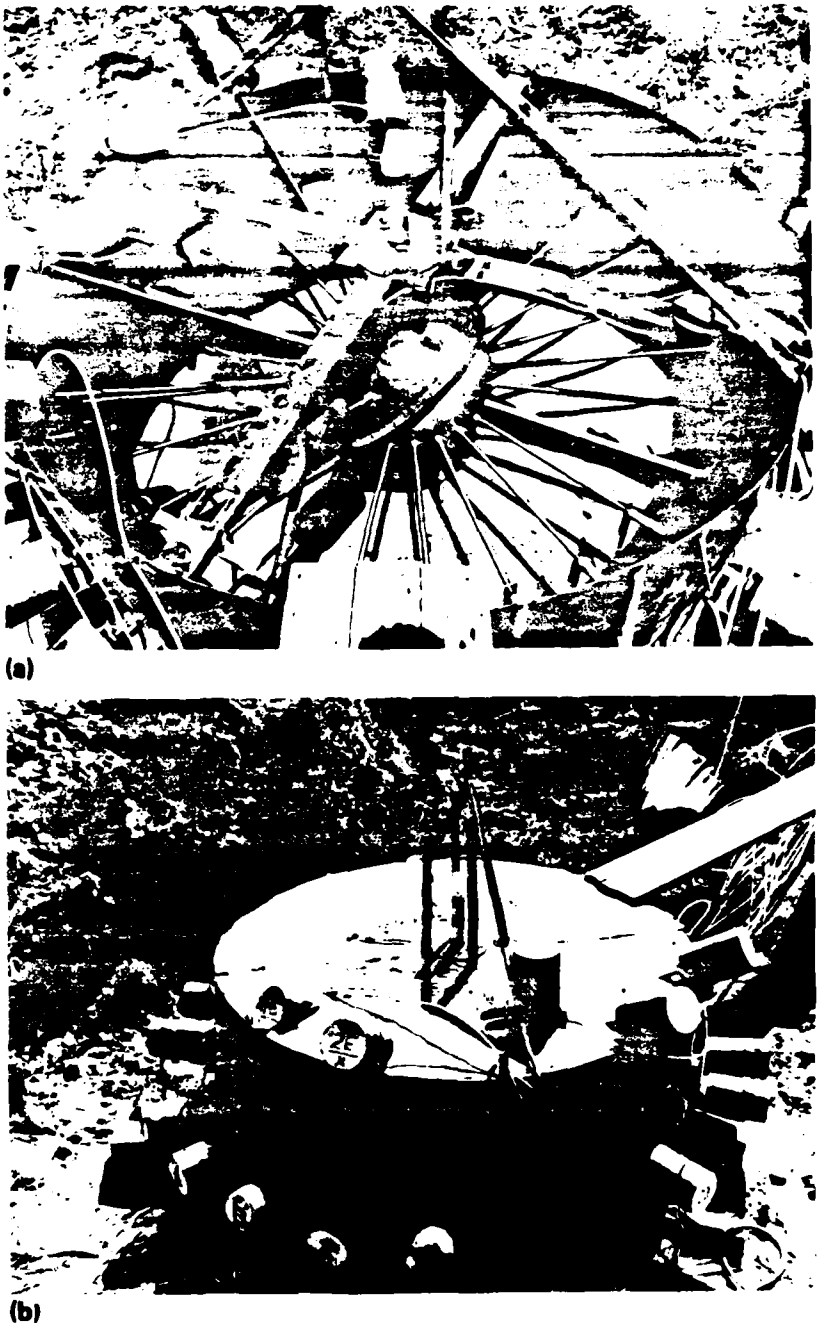

Figure 3 (a) Photograph of tank, explosive source, and LOS models; (b) photograph tank and aluminum targets after emplacement of saturated sand (LS-4). Tank diameter 2.44 m; diameter of sphere 61.0 cm

2.3 LOS MODEL DESCRIPTION

The LOS pipe models used in this experiment are listed in Table 1 and pictorially shown in Figure 4. The table provides a brief description of each model, its position in the test bed, the relevant dimensions of the models, and the salient dimensions of any asymmetries that were included in the model. The configuration and nomenclature for the helical and ring asymmetries used in this experiment are shown in Figure 5. The 26 models can be categorized according to technical objective in the following manner:

2.3.1 Reproducibility of Standard Models (Model 1 and 2). Models without asymmetries were designated as "Standard." Two of these models were included to compare the reproducibility of the jetting phenomena from these models and similar models tested in previous experiments.

2.3.2 Reproducibility of Models with Steel Helices (Models 3 and 4). A thin (0.5 mm) steel ribbon was located on the inside surface of these LOS models. Each ribbon was positioned to form a helix with a 50.8 mm pitch which would introduce asymmetries into the collapse process along the entire length of the model. Two of these models were used to verify reproducibility of this previously successful jet suppression technique.

2.3.3 Effect of Standard Models Containing Air (Models 17 and 19). In the previous experiment, LS-3, deeper and larger volume craters were observed when the tube thickness was

Table 1 Description of LOS pipe models tested in the LS-4 experiment

LOS Model	Model Position	Stainless Steel Tube Length[a] (mm)	Characteristics of Asymmetry or Other Jet Attenuation Method: Material	Width (mm)	Thickness (mm)	Length (mm)	Pitch/Spacing (mm)	Notes
Standard								
No. 1	1	994	--	--	--	--	--	
No. 2	2	994	--	--	--	--	--	
Full Length Internal Helix								
No. 1	3	994	Steel	15.9	0.5	981	51	
No. 2	4	994	Steel	15.9	0.5	981	51	
Full Length Wrap								
No. 1	5	994	Lead	--	2.03	994	--	
No. 2	7	994	Lead	--	2.03	994	--	
Flow Region Internal Helix								
No. 1	8	994	Steel	15.9	0.5	384	51	Used a helix in the last 384 mm of pipe
No. 2	9	994	Steel	15.9	0.5	384	51	
Flow Region Internal Rings								
No. 1	10	994	Lead	3.2	3.2	356	51	Lead rings spaced 51 mm apart in the last 356 mm of the pipe
No. 2	11	994	Lead	3.2	3.2	356	51	Same as No. 1
Expansion Chamber[b]								
No. 1 with Recessed Helix	15	610	Lead	3.2	3.2	384	51	Used helix inside expansion chamber in last 384 mm of tube (i.d. of helix was o.d. of LOS pipe)
No. 2 with Recessed Helix	16	610	Lead	3.2	3.2	384	51	Same as No. 1
No. 1 with Recessed Rings	13	610	Lead	3.2	3.2	384	0	Used rings spaced 51 mm apart the last 384 mm of the tube (i.d. of helix was o.d. of LOS pipe)
No. 2 with Recessed Rings	14	610	Lead	3.2	3.2	384	0	Same as No. 1

[a] 19 mm o.d., 0.3 mm wall thickness
[b] Chamber i.d. was 25.6 mm

Table 1 Description of LOS pipe models tested in the LS-4 experiment (cont.)

LOS Model	Model Position	Stainless Steel Tube Length[a] (mm)	Characteristics of Asymmetry or Other Jet Attenuation Method: Material	Width (mm)	Thickness (mm)	Length (mm)	Pitch/Spacing (mm)	Notes
Enhanced Jetting								
H.E. Products--Standard	20	953	--	--	--	--	--	Had NM in the first 38 mm of the tube length
H.E. Products--Helix	21	953	Steel	15.9	0.5	940	51	Same as HE Products--Standard but had a steel internal helix
Collapsed Pipe--Standard	2E[b]	1213	--	--	--	--	--	Had 216 mm of standard pipe inside the NM sphere
Collapsed Pipe--Helix	22E	1213	Steel	15.9	0.5	1200	51	Same as Collapsed Pipe--Standard but had an internal steel helix
1-atm Air								
Standard	17	994	--	--	--	--	--	Standard model at 1 atm internal air pressure
Standard with Helix	19	994	Steel	15.9	0.5	981	51	Same as Standard 1 atm model but had an internal helix the full length of the tube
Source Region Jet Characteristics								
10 cm Helix/100 cm Tube	22	994	Steel	15.9	0.5	305	51	Used a 994 mm standard tube with a helix in the first 300 mm of tube length
30 cm Helix/65 cm Tube	4E	664	Steel	15.9	0.5	305	51	Used a 664 mm standard tube with an internal helix in the first 300 mm of the tube
30 cm Helix/30 cm Tube	6E	318	Steel	15.9	0.5	305	51	Used a 318 mm standard tube with a helix (standard material and dimension) 300 mm of tube length
Helix to Expansion Chamber	18E	318	Steel	15.9	0.5	305	51	Used a 318 mm standard tube with a helix 305 mm long--allowed to expand into a chamber 102 mm dia x 89 mm deep
50 cm Standoff	20E	487	--	--	--	--	--	Tube began 500 mm from explosive sphere
90° Bend in Pipe	23	994	--	--	--	--	--	Tube had a 90° bend [radius = 18.7 cm] starting 300 mm from explosive sphere

[a] 19 mm outside diameter, 0.3 mm wall thickness
[b] E denotes an elevated LOS pipe model

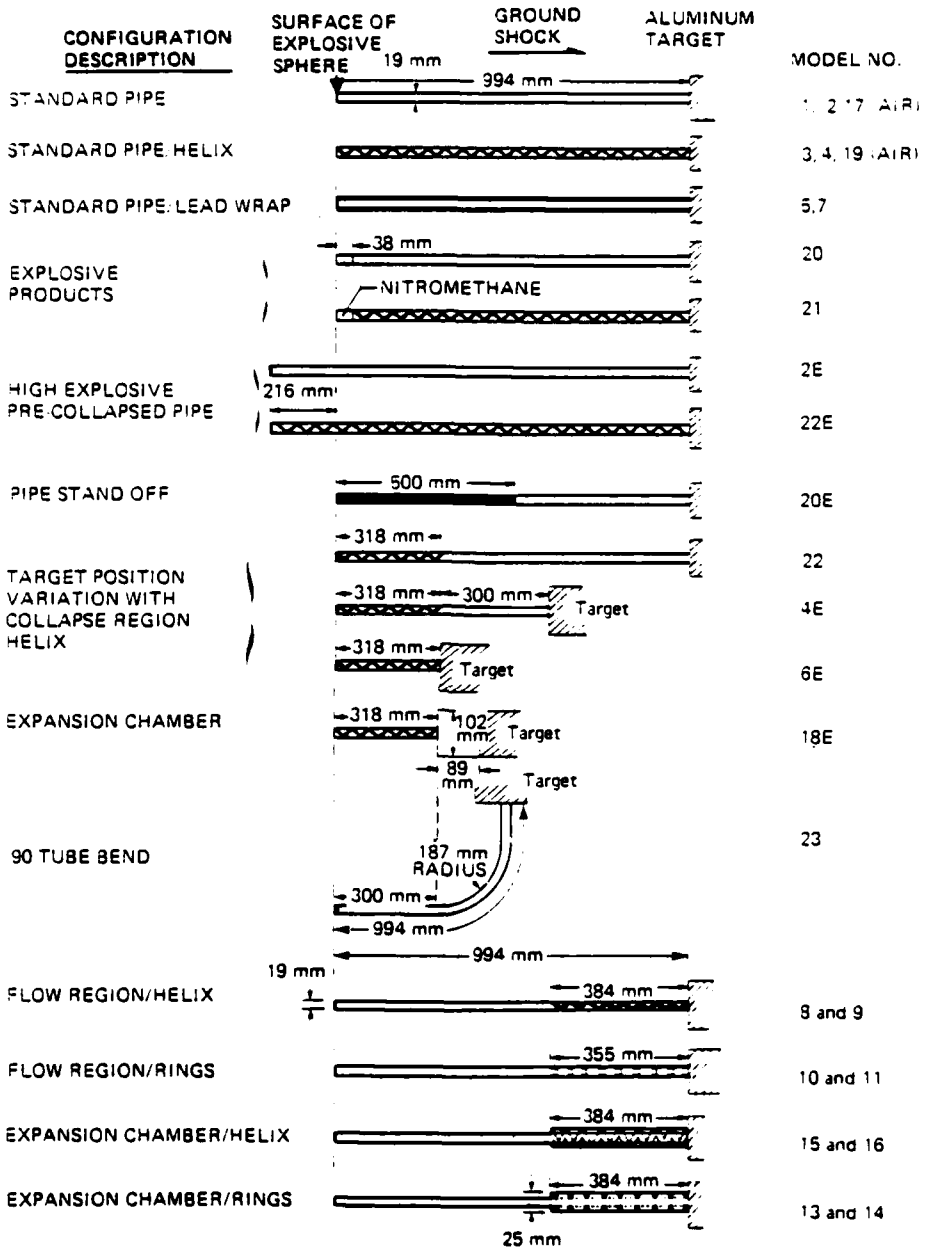

Figure 4 Pictorial configuration of models-used in the LS-4 experiment.

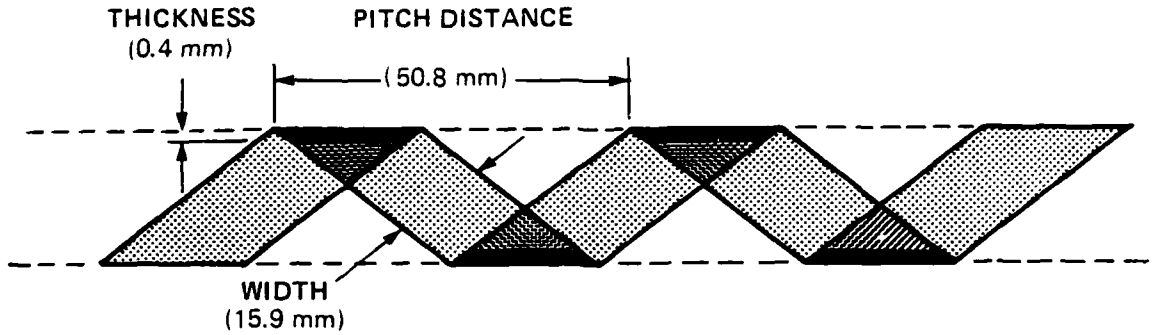

(a) Configuration of the standard helix asymmetry

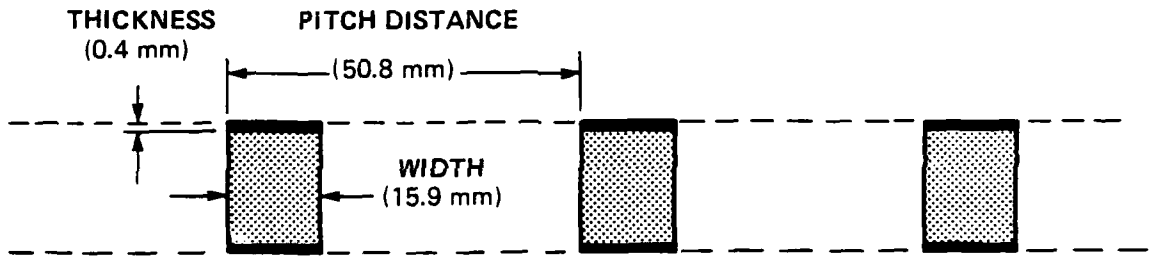

(b) Configuration of the standard ring asymmetry

Figure 5 Configuration and nomenclature of helical and ring asymmetries

increased from the standard of 0.31 mm to 0.71 mm by sliding a lead tube over the standard tube. In addition, these tubes contained one atmosphere of air (pinex models). To determine whether increased penetration was attributable to greater wall thickness (areal density increase) or to the presence of air, two standard-wall-thickness pipes containing one atmosphere of air were tested. Model 19 also incorporated a full-length helix to verify its effect in attenuating a jet.

2.3.4 Effect of LOS Tube Areal Density (Full-Length Lead Wrap Models 5 and 6). Two models (one with and one without a helix) were tested to further evaluate the effect of tube thickness or areal density in the formation of jets and craters. For these models, a lead tube with a wall thickness of 2 mm was slid over the standard tube to form a single composite tube with an outside diameter of 23 mm. The increase in the areal density changed from 0.24 gm/cm^2 for standard pipes to 2.51 gm/cm^2 for the lead wrapped model.

2.3.5 Explosive Products Models (Models 20 and 21). The first 38 mm of the pipe was open to the explosive sphere so it would fill with nitromethane explosive. When fired, this configuration should cause the end of the tube to flare and inject some explosive products into the tube. Whether this configuration would increase or decrease the amount of jetting was uncertain. One tube (Model 20) did not contain an asymmetry, while the other (Model 21) contained a standard full length helix.

2.3.6 High Explosive Precollapsed Pipes (Models 2E and 22E). For these models, the model lengths were increased 216 mm and this additional length of pipe was extended inside the explosive sphere, allowing this portion of the pipe to be collapsed by the full detonation pressure of the explosive prior to the normal tube collapse caused by ground shock in the sand. One tube had no asymmetry (Model 2E), while the other contained a helix the entire length of the pipe, including the portion extending inside the explosive sphere. Increased jet energy and deeper target penetration was anticipated, and it was uncertain that the helix would still be effective.

2.3.7 Pipe Standoff (Model 20E). To further evaluate the pipe length involved in the penetrating jet formation process and the data from the LS-3 experiment, the first 500 mm of a standard pipe was plugged with a nylon rod. This plug prevents the normal collapse of the pipe. In the LS-3 experiment, pipes with much shorter plugs were still forming crater producing jets.

2.3.8 Source Region Jet Characteristics (Models 22, 4E, and 6E). Three models were used to determine whether a short, 318-mm-long standard helix placed in the jet forming region of the pipe (nearest the explosive sphere) would prevent jet formation. The distance between the end of the helix and the model was also varied to determine the sensitivity of target penetration to this parameter.

2.3.9 Effect of an Expansion Chamber (Model 18E). Model 18E was designed to evaluate whether an expansion chamber added to the end of a short pipe would alter the jet by allowing it to expand radially before reaching the target.

2.3.10 Flow Region Asymmetries (Models 8, 9, 10, and 11). These models were designed to further evaluate the effect of asymmetries placed in the flow region. The region of the pipe beyond which no jet forms is defined as the flow region. Model 12 in LS-3 used a thick lead helix in this region and was very effective in reducing the jet, but it was not known if a thin steel helix would also be effective. In two of the models (8 and 9), standard helices were placed inside the pipe for only the last 384 mm of the standard 994 mm pipe length. This position should be well beyond the jet generating region of the pipe. To evaluate whether rings are also as effective as helices in attenuating jets, Models 10 and 11 contained standard rings in the last 355 mm of pipe length.

2.3.11 Flow Region Asymmetries Contained in Expansion Chambers (Models 13, 14, 15, and 16). Since mufflers are sometimes used on UGT LOS designs, expansion chambers were added to the last 384 mm of four models to represent a muffler configuration. Both thick rings and thick helices were placed in the expansion chamber to evaluate their effect on attenuating the jetting flow. The inside diameter of the rings and helices was the same as the pipe inside diameter.

2.4 MEASUREMENTS

The active instrumentation used in this experiment was directed at determining the time at which the detonation reaches the inside surface of the fiberglass sphere, the trajectory of the spherically divergent shock wave in the saturated sand, pressure generated inside the models, the velocity of the jets generated in four of the LOS models, and the rate at which the jet penetrates the aluminum target of several models. Carbon stress gages were also embedded in selected targets.

Aluminum targets were placed at the end of all models to provide passive, terminal evidence of the energy and momentum contained in the jet.

Table 2 summarizes the instrumentation used on the various models of this experiment.

2.4.1 Detonation Wave. Four ionization pins were located on opposite sides of the explosive sphere. They were positioned on the inside surface of the fiberglass sphere to measure the time at which the detonation wave reaches this interface. The purpose of this measurement was to assure that the detonation was spherically symmetrical about the point of initiation prior to entering the saturated sand surrounding the models.

2.4.2 Shock Wave in Test Bed. The trajectory of the spherically divergent shock wave in the saturated sand test bed was determined from time-of-arrival measurements. These measurements were obtained from the response of two radial lines

Table 2 Summary of instrumented LOS pipe models for LS-4.

LOS Model Name	Model Number and Position	Pipe Jet Velocity	Aluminum Target Impact Switch	Stagnation Pressure at the Target	Target Penetration Pins	Stress Gage in the Target
Standard 1	1	5 ionization pins	double foil	quartz gage	7 shorting	two piezoresistive
Standard 2	2	--	double foil	quartz gage	7 shorting	--
Helix 1	3	5 ionization pins	double foil	quartz gage	--	two piezoresistive
Helix 2	4	--	double foil	quartz gage	--	two piezoresistive
Lead Wrap 1	5	5 ionization pins	double foil	quartz gage	7 shorting	two piezoresistive
Lead Wrap 2	7	--	double foil	quartz gage	7 shorting	--
HE Precursor	20	5 ionization pins	double foil	--	--	--
Jet Precursor	2E	--	double foil	--	--	--

of seven piezoelectric pins placed in the saturated sand on opposite sides of the explosive sphere. They were located in the horizontal midplane of the sphere and extended from 32.5 cm to 107.5 cm from the center of the sphere. The first piezoelectric pin of each radial line was located 2.0 cm from the inside surface of the explosive sphere. The intervals between the first and second pin and between the second and third pin were 5 cm and 10 cm, respectively. Thereafter the interval between pins was 15 cm.

2.4.3 Jet Velocity. Instrumentation for determining jet velocity was included on four models: the standard (Model 1), the model with a helix (No. 3), and the two models with lead wraps (No. 5 and 7). The instrumentation consisted of five ionization pins placed through the walls of the models at 5-cm intervals and extending from 65 cm to 85 cm from the steel plug on the end of the model nearest to the explosive sphere. The geometry for the ionization pin instrumentation is shown in Figure 6 along with a photograph of a tube with the pins attached.

Impact switches attached to the front of eight targets measured TOA of the ionized gas flow and the subsequent flow that produced target damage. These switches consisted of a sandwich of two aluminum foils separated by thin Mylar sheets. A 6-mm-diameter hole was cut in the first Mylar sheet, exposing it to the LOS pipe interior so that any ionizing flow would short out the charged foil to the pipe wall, producing a signal. The second foil does not produce a signal until the 0.076-mm thickness of Mylar is penetrated. The configuration of these impact switches is shown in Figure 7.

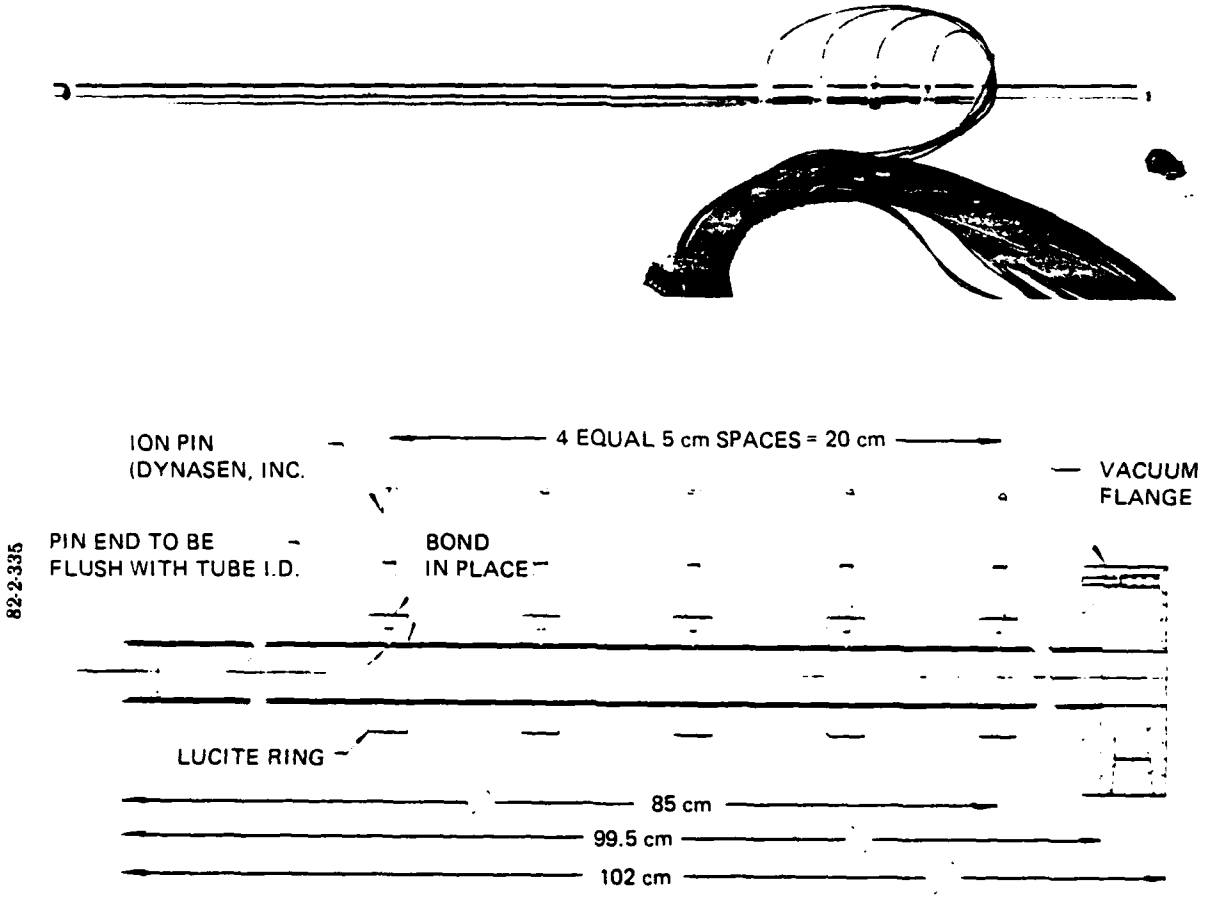

Figure 6 Configuration of ionization pins used for jet velocity inside the LOS tubes.

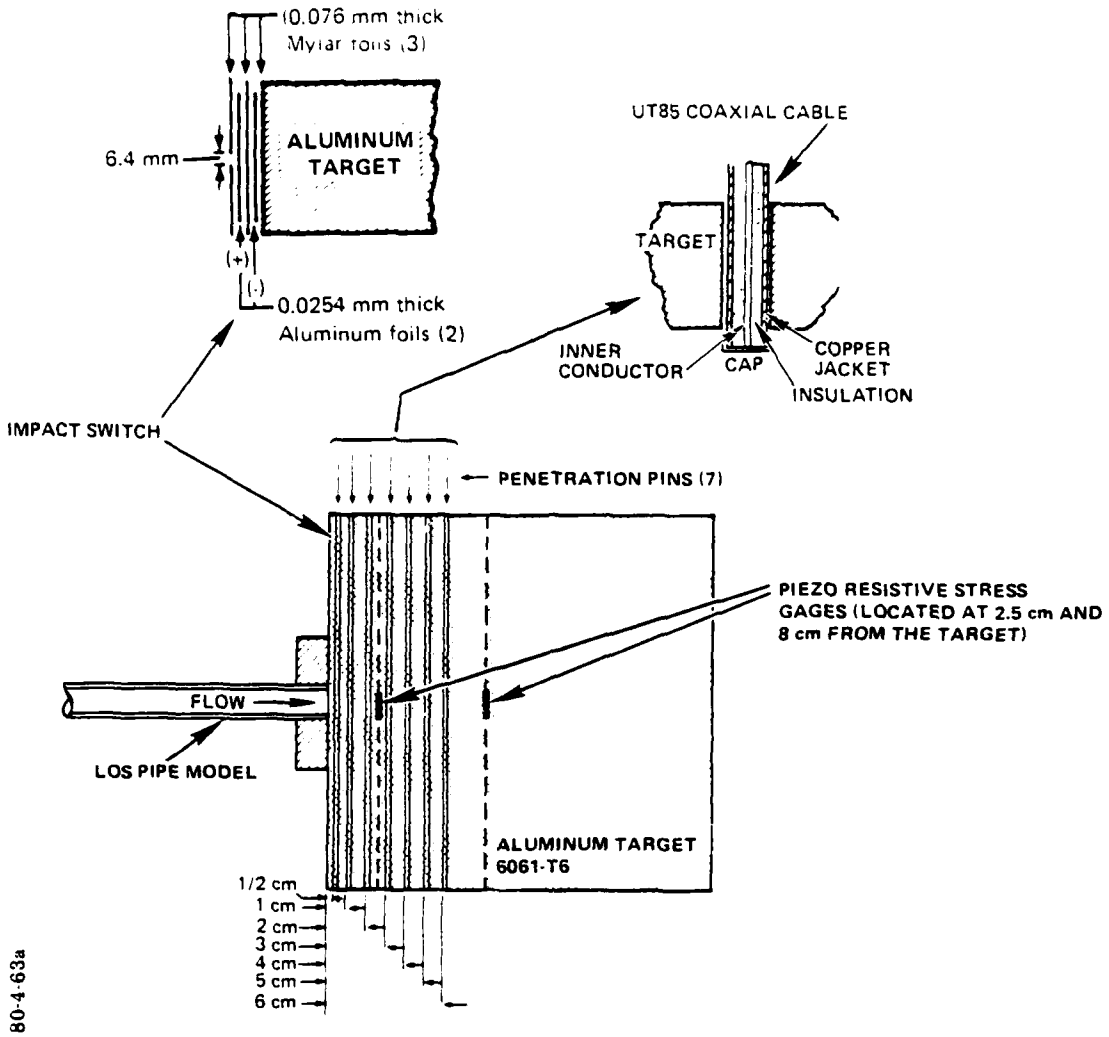

Figure 7 Instrumentation used for measuring the jet TOA at the target face and jet penetration and stress within the target

2.4.4 Jet Pressure. To measure the magnitude of the pressure generated by the flow within the pipe, pressure gages were placed in the target mounting flange (see Figure 8). A 5-cm column of oil separated the gage from the inner pipe wall for ease of mounting and to provide temperature and shock isolation. The 13-mm gage port distance from the target face allows observation of the pressure wave before and after reflection from the target face. The gage used for these measurements was a PCB Model 109A piezoelectric pressure gage* (PZ gage) with a dynamic range of 0 to 550 MPa (0 to 5.5 kbar).

2.4.5 Rate of Target Penetration. Using the configuration shown in Figure 7, the aluminum targets of eight LOS models contained TOA instrumentation to investigate the rate of jet penetration. Six UT 85 coaxial cables were placed in small tight-fitting holes drilled through the centerline of the target. Successive coaxial cables short out as the jet penetrates the target.

2.4.6 Stress Inside Target. Carbon gages were placed inside four aluminum targets to measure the transmitted impact stresses. These were 50 Ω model C-300-50-EC carbon gages.** The gages are supplied with a pulsed constant current and the voltage change is recorded when the gage resistance changes with stress. One gage was located on the pipe axis at a depth of 2.5 cm from the front face of the target. For those targets with two gages, the second was located 8 cm from the front face. The targets

*Manufactured by PCB Piezotronics, Buffalo, NY
**Manufactured by Dynasen, Inc., Goleta, CA.

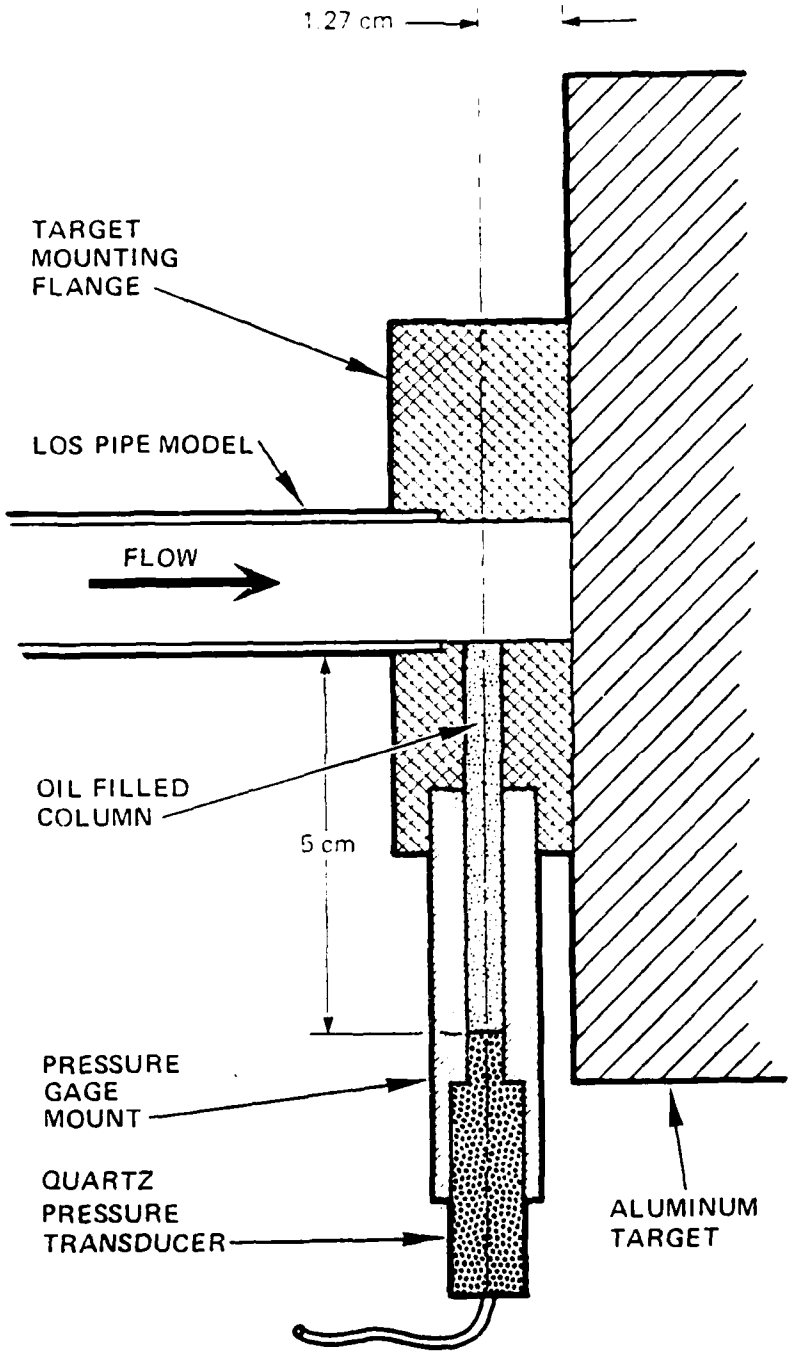

Figure 8 Configuration of typical pressure gage mount

were of a laminated construction and these thin gages were positioned at the interfaces of the target with epoxy.

2.4.7 Target Damage. Measurement of the depth and diameter of the craters produced in aluminum targets provided passive evidence of the energy and momentum in the jets. The targets were 20-cm-diameter 6061-T6 aluminum cylinders with a length of 30 cm. They were supported on brackets welded to the outside of the steel test bed tank and positioned against the vacuum flange that enclosed the exit end of each LOS pipe model.

SECTION 3

EXPERIMENTAL RESULTS

3.1 DETONATION WAVE

The two ionization pins on the inside surface of the fiberglass sphere showed a 0.5 μs difference in the times at which the detonation wave arrived at four sides of the sphere. Assuming the detonation velocity in the nitromethane was 0.6 cm/μs, a 0.5 μs difference in arrival times would imply that the detonation wave on one side of the sphere was leading the opposite side by 0.3 cm. Since the fiberglass sphere had an internal radius of 30.6 cm, this represents a difference of one percent. This difference is probably due to the inability to maintain the shape of the thin-walled fiberglass sphere when it is filled with 136 kilograms of a liquid and covered with saturated sand. Therefore, for all practical purposes, the detonation was quite symmetrical.

3.2 SHOCK WAVE IN TEST BED

The time-of-arrival data for the spherically divergent shock wave along the two PZ pin diagnostic lines are shown in Figure 9. The data for the two lines are almost identical, providing good confidence in the values obtained even though the signals were somewhat noisy, with multiple reports in many cases. As can be seen, only four of the seven pins gave signals

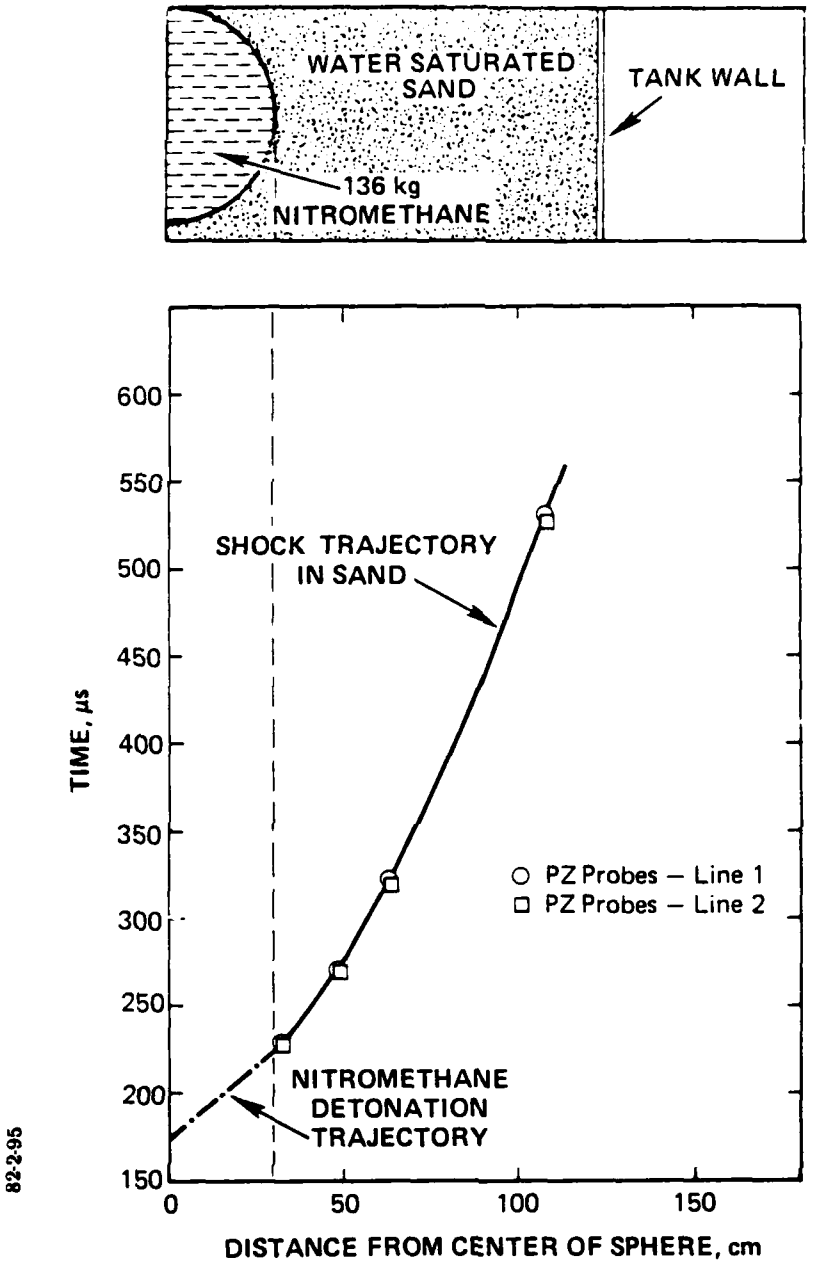

Figure 9 Shock trajectory in saturated sand of Test LS-4

that were clearly identifiable. The data suggest that the test bed was fully saturated and was similar to the LS-2 and LS-3 experiment test bed data shown in Figure 10.

3.3 JET VELOCITY

The time-of-arrival (TOA) data obtained from the ionization pins located in the sidewalls of the four models with this instrumentation were almost uninterpretable. The signals were polarity coded, but in many cases the signals were recorded out of sequence. The trajectories of the best estimated data for the four models with jet velocity pins are shown in Figures 11 through 14. The target foil switch data is also shown in these plots. Most of the target switch data, however, was lost due to shorts in the switches caused by mechanical damage during the test setup.

The shock trajectory of 1.2 cm/μs obtained for Model 1 (Standard No. 1) was somewhat higher than the velocities estimated for the four standard models in the LS-2 experiment from the target ionization TOA data which lay between 0.85 and 0.97 cm/μs. The velocities obtained for Model 3 (Helix No. 1) and Model 20 (H.E. precursor) were both 0.94 cm/μs. Model 5 (lead wrap No. 1) gave a velocity of approximately 0.84 cm/μs. The apparent origin of the jet was near the pipe-explosive sphere interface for Models 1, 3, and 5.

The origin for Model 20, which had nitromethane explosive extending into the first 3.8 cm, was located approximately 8 cm into the sand of the test bed. Since the short column of

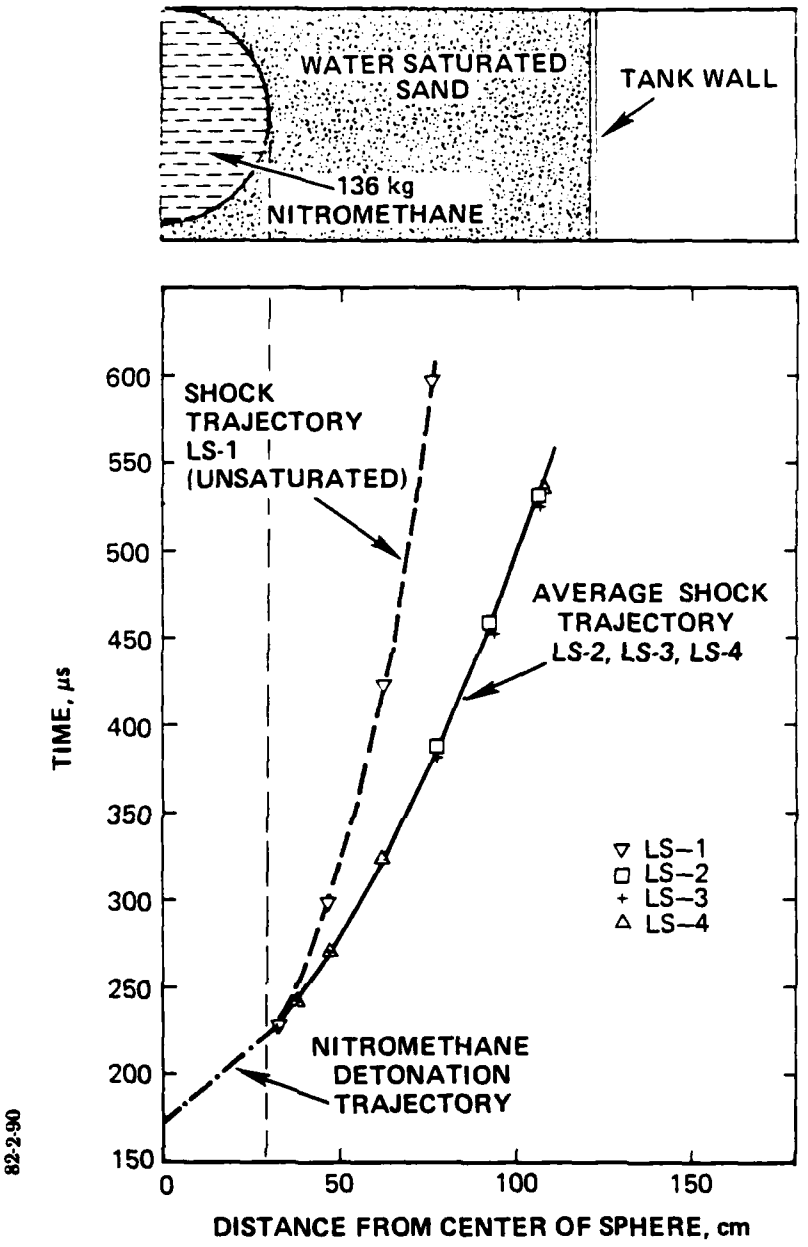

Figure 10 Comparison of shock trajectories in sand from Tests LS-1, LS-2, LS-3, and LS-4

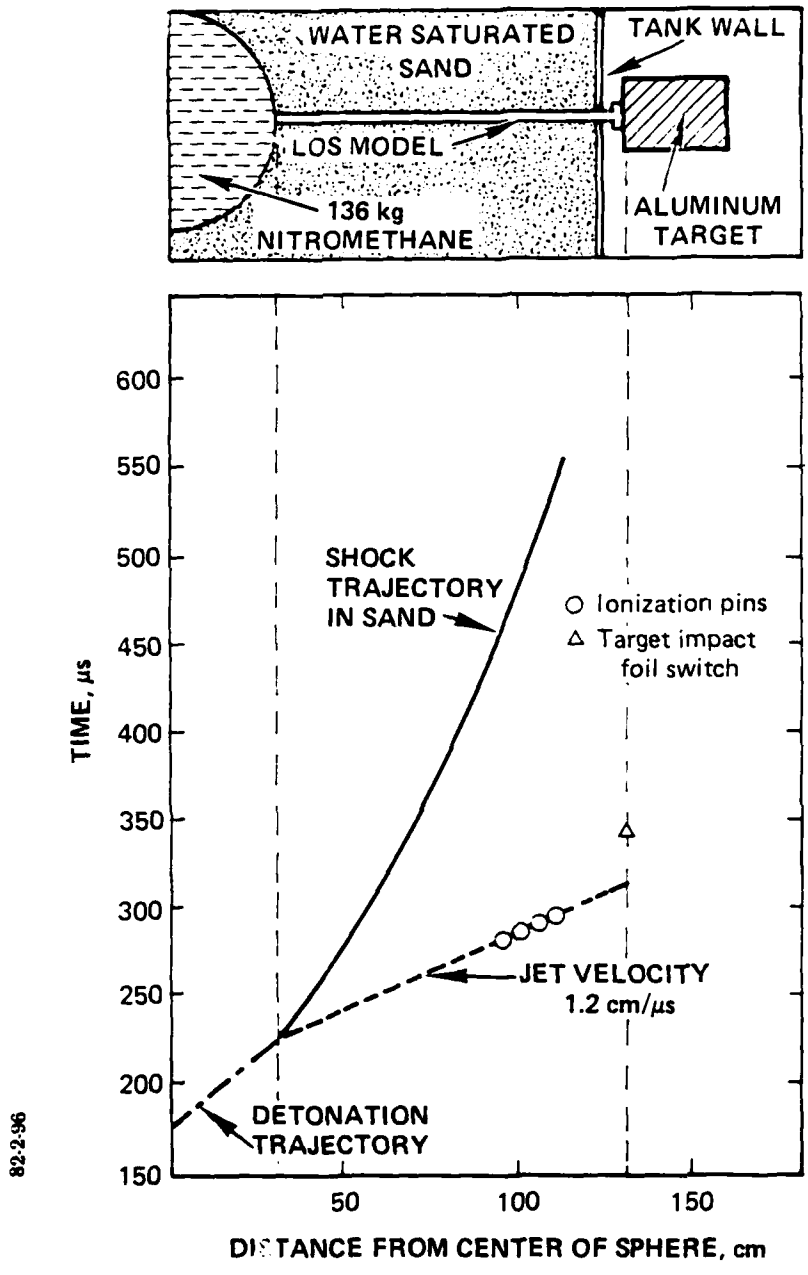

Figure 11 Jet trajectory from ionization pins for Model 1 (Standard No. 1)

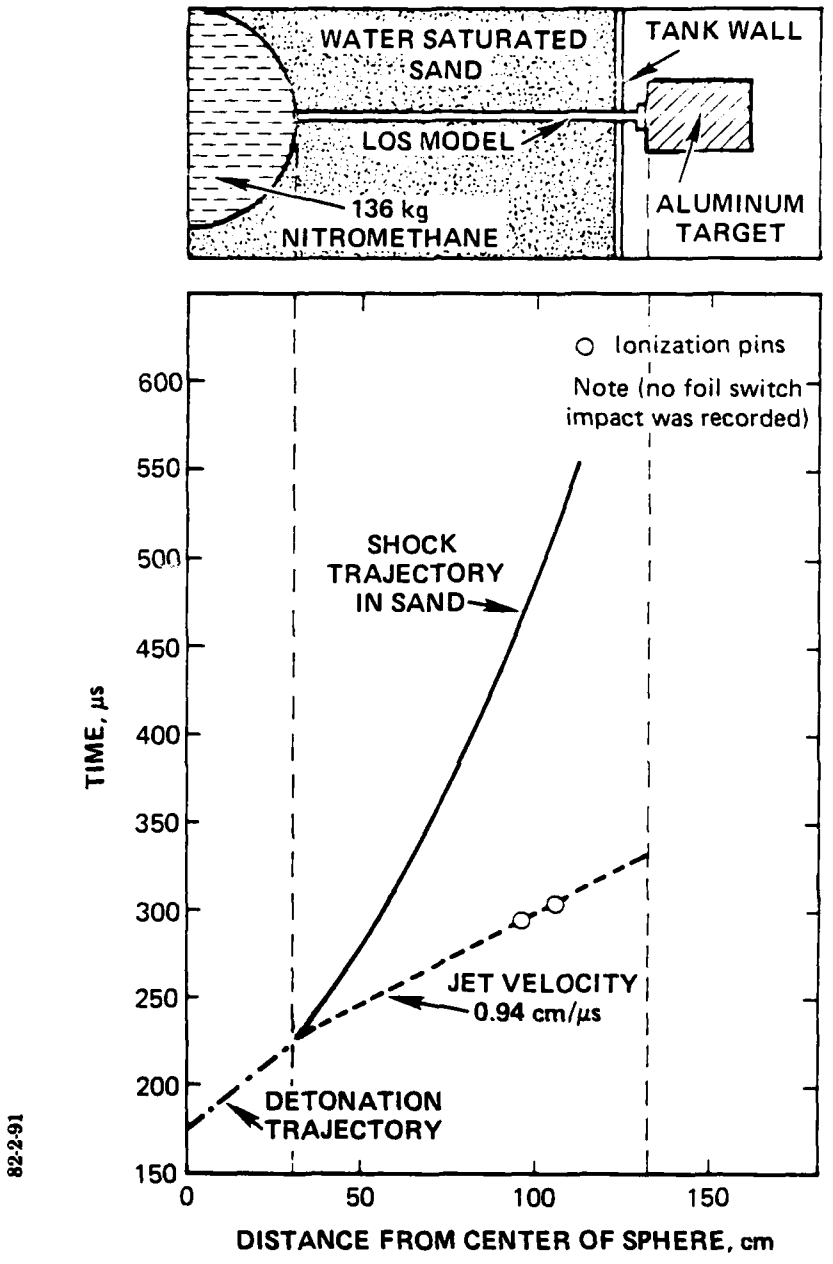

Figure 12 Jet trajectory from ionization pins for Model 3 (Helix No. 1)

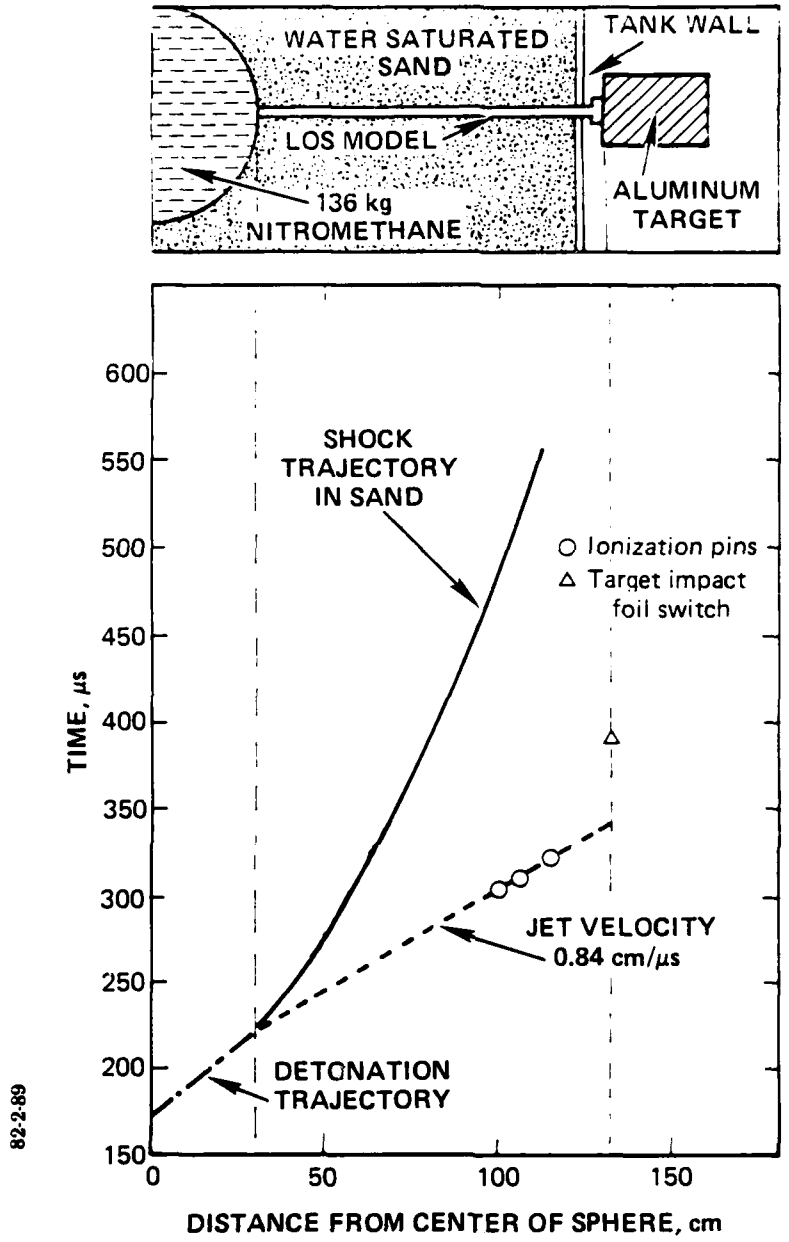

Figure 13 Jet trajectory from ionization pins for Model 5 (lead wrap No. 1)

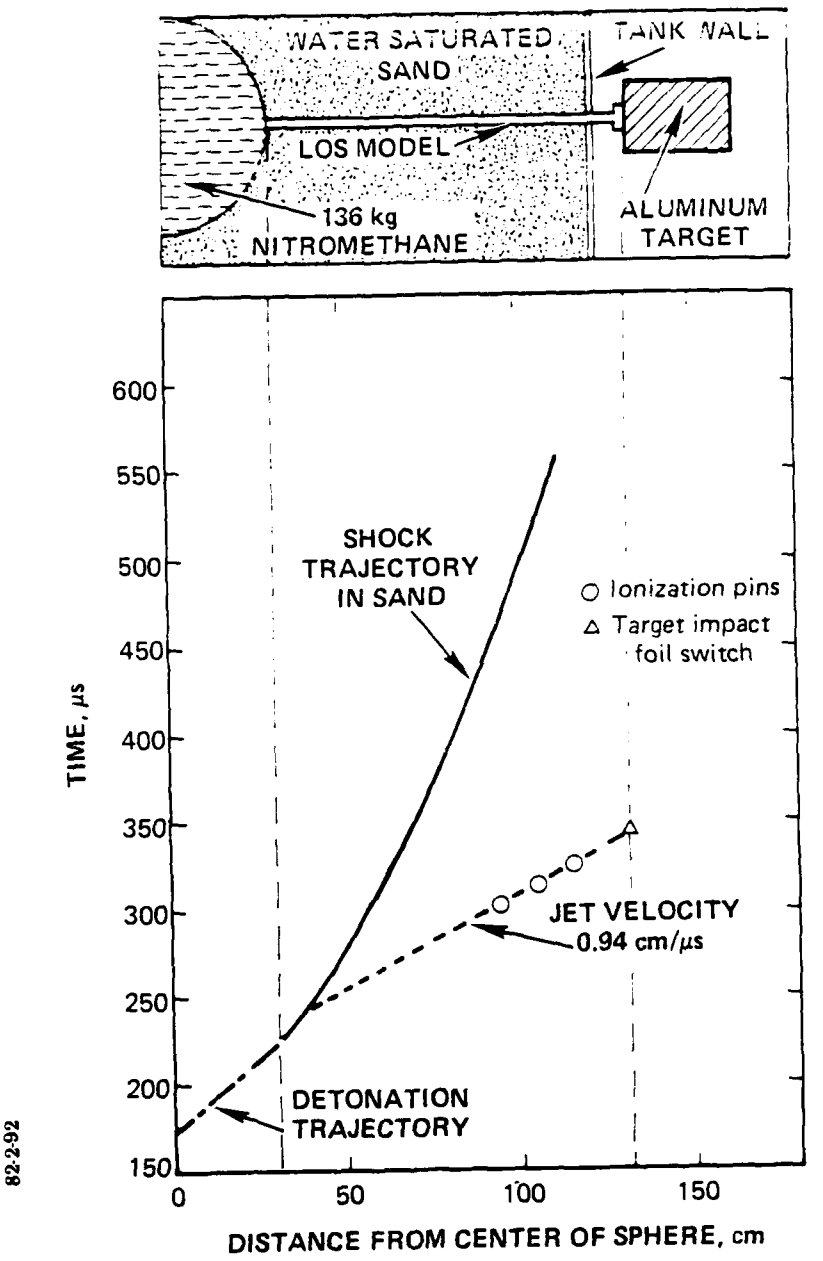

Figure 14 Jet trajectory from ionization pins for Model 20 (H.E. precursor)

explosive would flare the tube end for some distance, this change in apparent collapse origin is not surprising.

3.4 JET PRESSURE

The quartz pressure gage records obtained from six gages, each located in front of different targets, are shown in Figure 15. The length of time that valid pressures can be recorded is dependent both on the time required for the LOS model pipe to rupture and time of separation of the target flange from the aluminum target. Wall thickness of the pipe used permitted rapid expansion with pressure. In addition, the method of attaching the pipe to the target allowed separation and pressure loss with even slight movement of the pipe or target. There may also be other pressure loss mechanisms. For these reasons, no estimate of valid recording time can be made. The pressure signals are also delayed approximately 50 μs by the transit time of the 5-cm-long oil-filled column.

The signals recorded for Models 1 and 2 (standard pipes with no asymmetries) are reasonably different in character. The gage on Model 1 shows a negative pressure of about 0.5 kbar on the first large peak (which is impossible), suggesting that the gage is not validly recording at that time or almost certainly is not at later times. The signals from the gages on the other models also show large negative pressures or unusual character which suggest that the values recorded beyond the major pressure spike should be evaluated with caution.

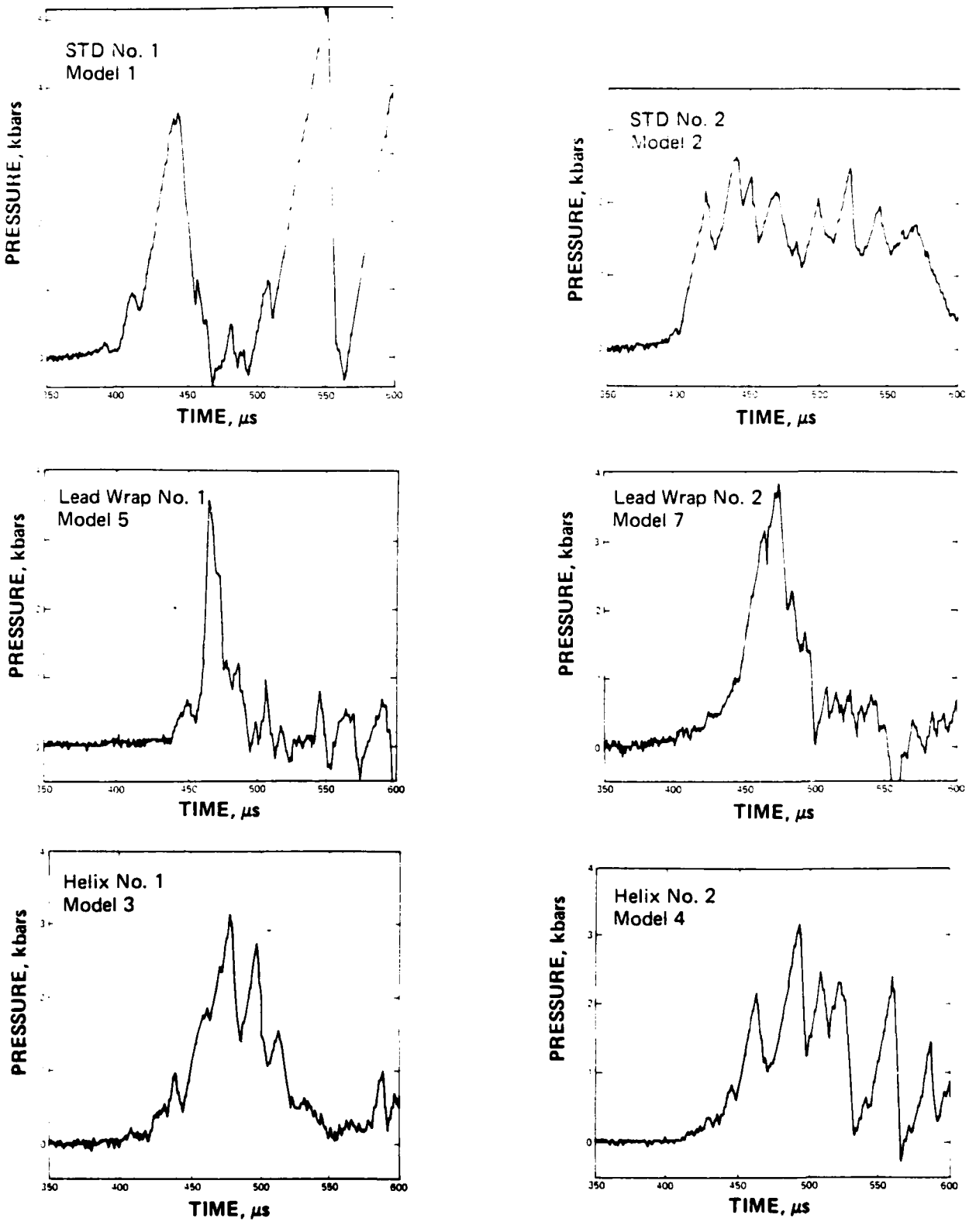

Figure 15 Quartz pressure gage records obtained in front of the targets for LS-4

There appears to be reasonable correlation between the onset of recorded pressure and the projected arrival time of the initial jet at the target obtained from the ionization pin data along the model tubes. There does not appear to be a significant pressure pulse occurring at the time of gas jet arrival but rather a slow increase in pressure. This onset of pressure is where the signal shows a slow, slight rise from the baseline. For Model 1 (standard), the onset of pressure occurs about 315 μs after correcting for the 50 μs transit time of the oil column, while the projected jet arrival time from Figure 11 is also 315 μs. For Model 3 (helix) the pressure onset occurs at a corrected time of 380 μs and the projected jet arrival time is 383 μs (Figure 12). Model 5 (thick lead wrap) shows a pressure onset at 337 μs and a projected jet arrival time of about 344 μs (Figure 13). Since there is no significant pressure recorded at this time, the data suggests that the initial high velocity jet (~ 0.84 to 1.2 cm/μs) does not produce high pressure and is not contributing to the penetration process, as will be further confirmed from the target penetration data which is discussed next.

There does at first appear to be a correlation between the first major pressure peak and the start of target penetration. However, the peak also appears when there is no penetration. For example, the pressure records for the models with helices showed very similar pressure peaks around 3 to 4 kbars, even though there was no penetration for these targets. The source of the pressure pulse has not been identified and further investigation of these gages and their mounting needs to be addressed before significant credibility can be given to the pressure signatures.

3.5 RATE OF TARGET PENETRATION

The rate of target penetration was measured with small diameter coaxial pins inserted into the target. Of the four instrumented targets, three provided good data while the data from the fourth was lost due to a malfunctioning oscilloscope.

Deep penetrations were recorded from the two lead wrapped models (Models 5 and 7) and showed quite linear penetration velocities of 0.058 and 0.062 cm/μs. These data are shown in Figures 16 and 17. The linear character of the penetration rate suggests that the penetration process occurs as a series of discrete or continuous impacts that occur over a rather long duration as opposed to a large, single impact. Observations of the target damage shown later also confirm this suggestion.

The third set of data, also shown in Figure 16, are from the Model 1 target (standard) which had a measured total penetration depth of 4.1 cm. These data also show a linear initial penetration for about 2 cm before showing a velocity decrease. The slope of this trajectory was about 0.068 cm/μs, similar to the rates from the other two targets.

Figures 17 and 18 show shock, jet, and penetration trajectories recorded for Models 1 and 5. The average penetrating jet velocity was obtained by using the time of target penetration and assuming that the jet starts at the assumed origin of the gaseous jet. This time of jet flight through the pipe length yields identical velocities of 0.53 cm/μs for lead wrapped models

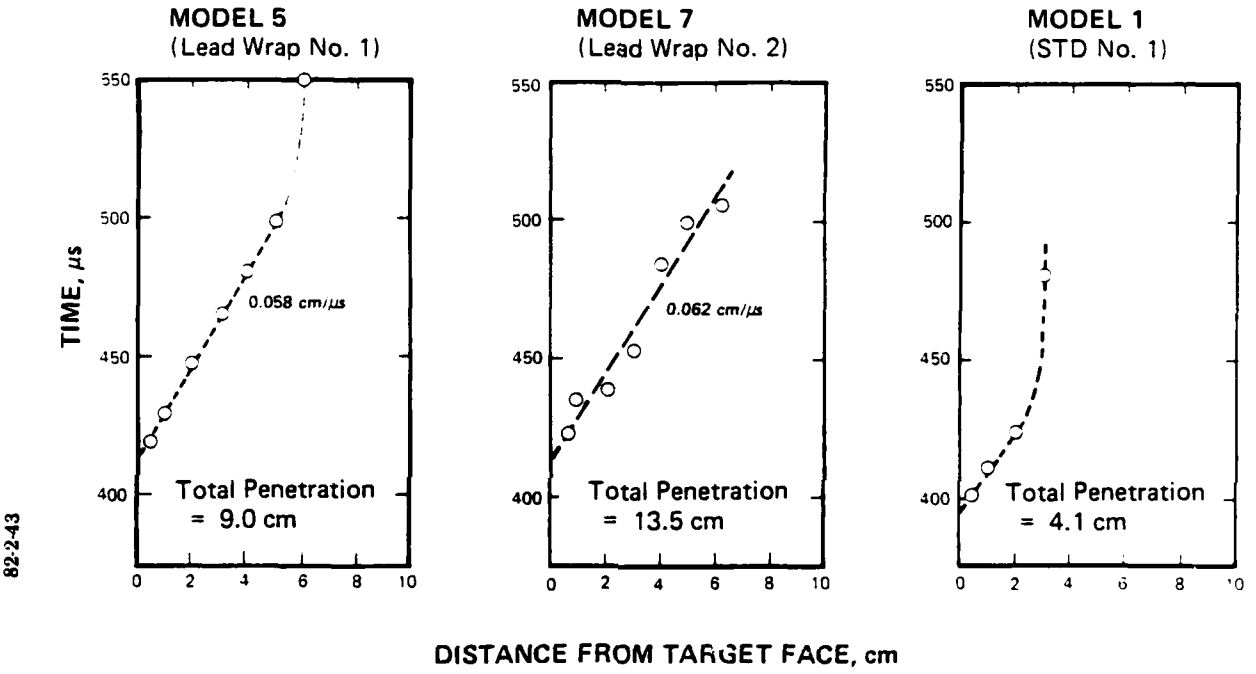

Figure 16 Comparison of target penetration data for Model 5, Model 7, and Model 1 of LS-4

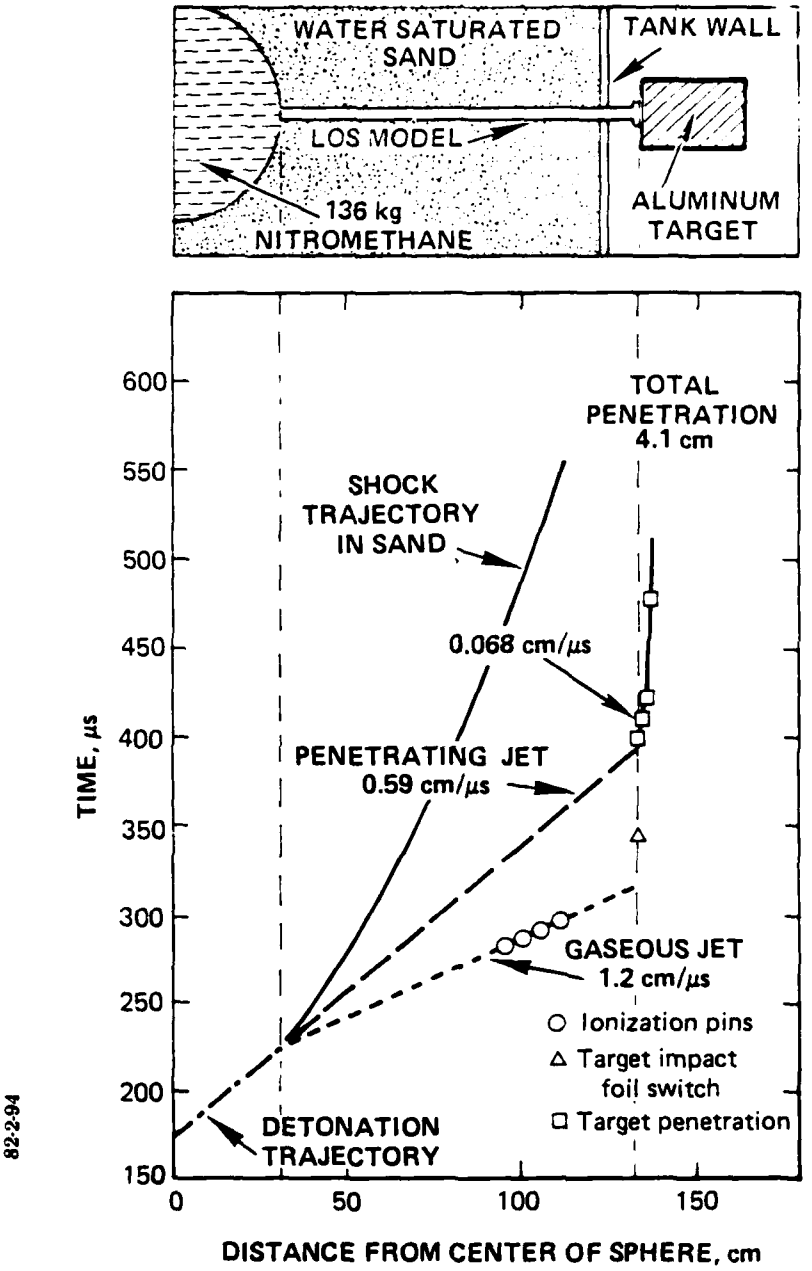

Figure 17 Shock, jet, and penetration trajectories for Model 1 (Standard No. 1), Experiment LS-4

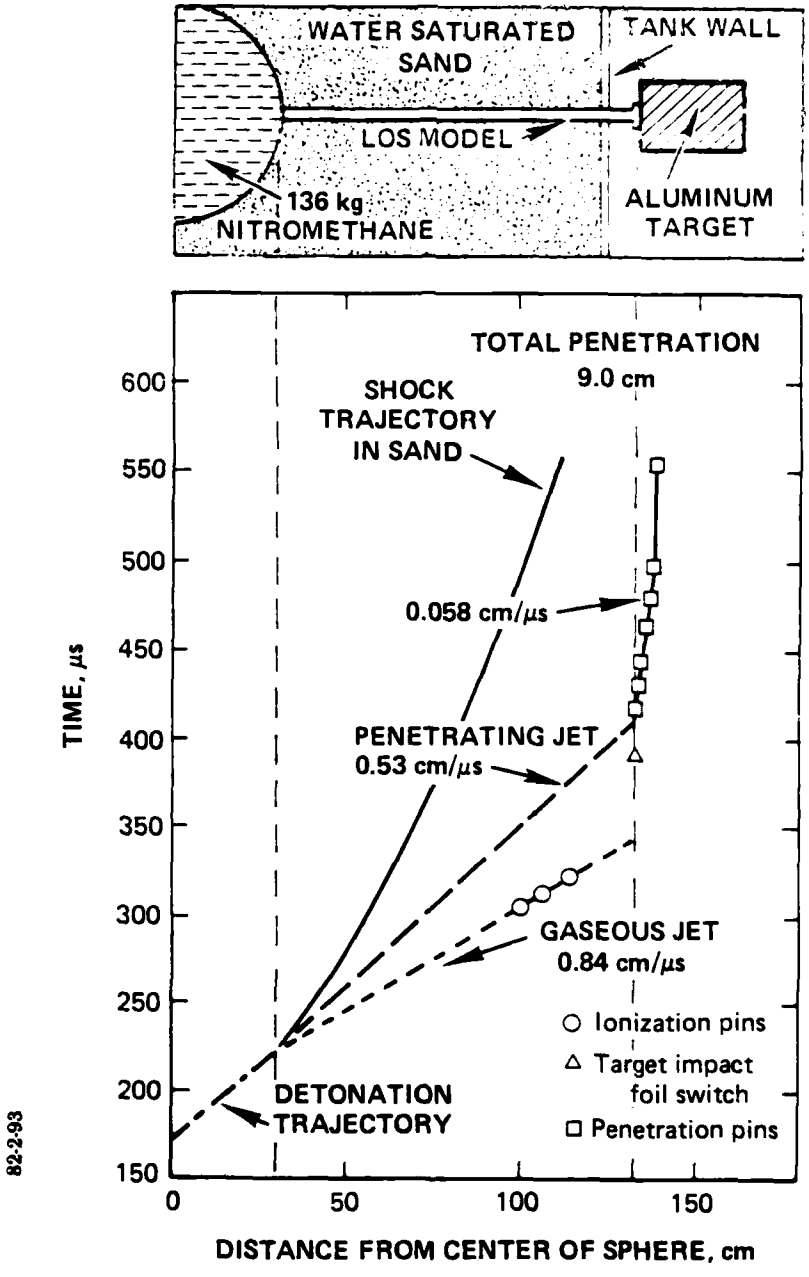

Figure 18 Shock, jet, and penetration trajectories for Model 5 (lead wrap No. 1), Experiment LS-4

(Models 5 and 7) and 0.59 cm/μs for the standard model. This value of 0.59 cm/μs for the standard model is consistent with the 0.62 cm/μs velocity obtained for the Model 4 (standard) in experiment LS-3.

3.6 TARGET STRESS GAGES

The target stress was measured with piezoresistive carbon gages embedded in four aluminum targets at 2.5 cm and 8 cm from the target face. The records for those gages are shown in Figure 19. The initial spike shown on each gage at 350 μs is caused by the current surge when the pulsed constant current supply for these gages was turned on.

For the Model 1 target (standard), the stress signal begins to rise at about 402 μs when the penetrating jet approaches the gage at about a tenth of the sound speed of aluminum. At 425 μs the pressure is about 4 kbars and the slope of the signal increases dramatically until the upper limit of the gage's response is reached, which is about 45 kbars. We suspect that the penetrating jet destroys the gage where the slope change in the signal occurs, although there is no conclusive proof. The second gage was located at 8 cm and beyond the total jet penetration depth of 4.1 cm. In this case, the maximum stress recorded is less than 0.5 kbars and the stress signature may be somewhat questionable at these low values due to gage heating.

The records from the two gages in the target of Model 5 are both quite similar in character. The signal increases starting at 432 μs shows a dramatic slope change at 449 μs when the

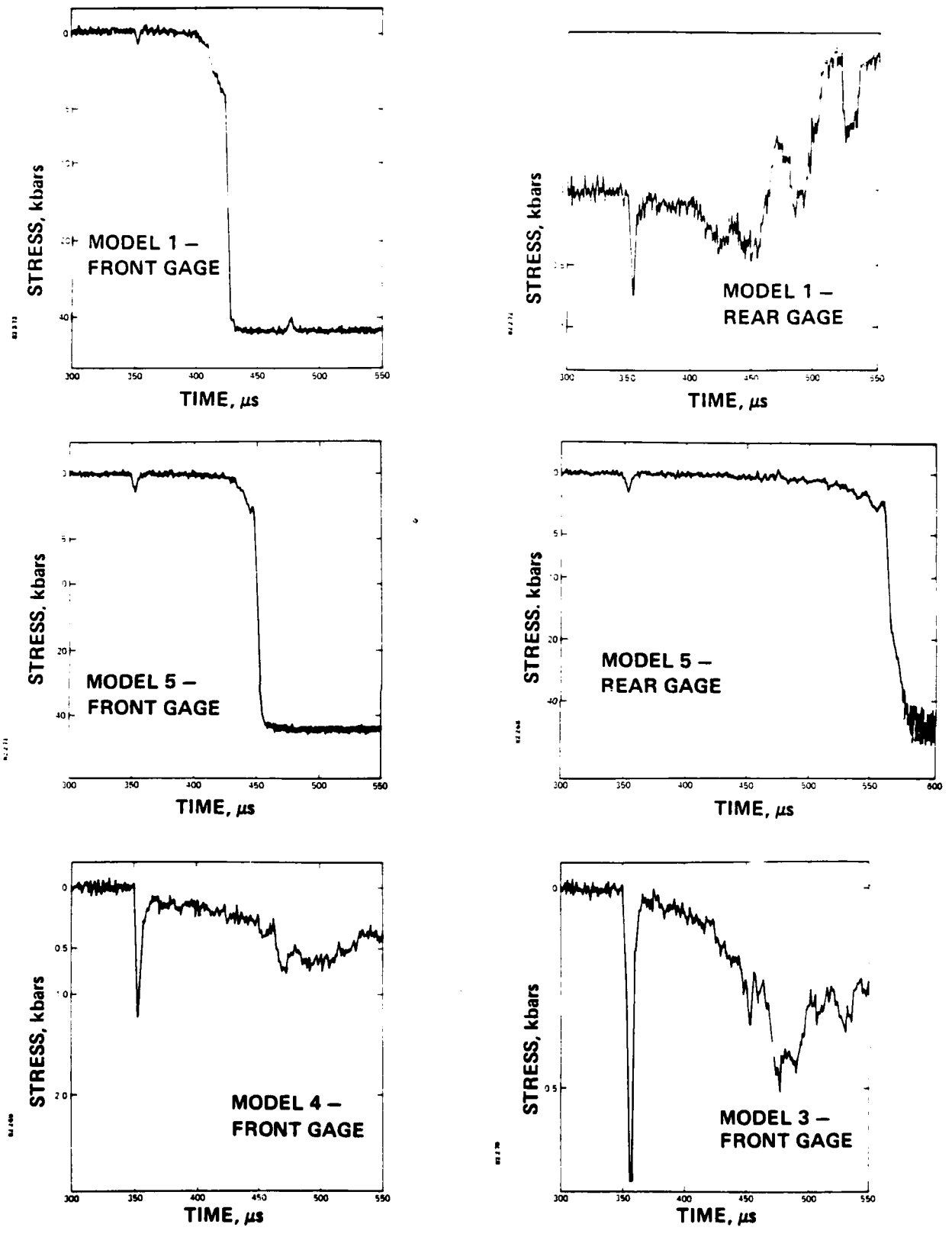

82-3-137

Figure 19 Records of carbon stress gages embedded in four aluminum targets for LS-4

pressure is approximately 3 kbars, and then rapidly reaches maximum signal. The second gage for this target was also penetrated and shows the same characteristics as exhibited by the front gage.

On the targets for Models 3 and 4 only the front gages were used because we did not anticipate any target penetration. The signals seem to confirm this fact and only show amplitudes of about 0.5 kbars, some of which may be due to gage heating.

When comparing these data with the penetration pin data we see that the slope change tends to occur at a slightly earlier time than we would predict from the average penetration data. This discrepancy leaves somewhat unresolved whether the gage signal saturates before the arrival of the penetrating jet, whether the penetration pins are slow to respond (which is unlikely), or whether the carbon gage data is just at the lower error bound of the penetration data.

No large-amplitude signals are observed which could be related to the arrival time of the initial gas jet. In a few cases, however, the turn-on time for the power supplies was unfortunately very similar to the arrival time for the gas jet.

3.7 TARGET DAMAGE

The recording of aluminum target damage, as in previous experiments, provides the best measurement of whether an asymmetry in an LOS model design has defeated the penetrating jet. A

summary of the measured penetration depths and volumes are shown in Table 3.

Four of the 26 targets fielded were not recovered, including three targets which were elevated above the midplane of the test bed in order to insert them into the already designed experimental arrangement. Even targets that were positioned horizontally were recovered well over 300 m from the test location. Tall grass, ravines, and uncertain flight trajectories contributed to the unfortunate loss of these targets. The penetration craters in the recovered targets were measured, sectioned, and photographed.

3.7.1 Standard Model Reproducibility (Models 1 and 2). The depths of penetration in the two targets from Models 1 and 2 were quite comparable at 4.1 cm and 4.0 cm; but the volumes were substantially different, with 14.8 cm^3 for Model 1 and 9.0 cm^3 for Model 2. Photographs of these targets are shown in Figure 20. The depths were just within the standard deviation of 1.15 cm for a mean depth of 5.15 cm recorded for six similar targets from the LS-2 and LS-3 experiments. The volumes were beyond one standard deviation of 8.7 cm^3 for a mean of 19.8 cm^3 determined from previous targets. No complete explanation is available for such penetration variations observed from supposedly identical models, but we presume it may be attributable to the sensitivity of the jet formation process to such factors as minor thickness variations of the LOS pipe.

3.7.2 Reproducibility of Models with Steel Helices (Models 3 and 4). As in all previous tests, models containing an

Table 3 Summary of target damage resulting from the various LOS models used in Experiment LS-4.

LOS Models Designated by Type	Model No. and Position	Penetration Depth (cm)	Hole Volume (cm³)	Notes
STANDARD MODELS				
No. 1	1	4.1	14.8	
No. 2	2	4.0	9.0	
HELICAL MODELS				
No. 1	3	< 0.1	< 0.1	Pitted surface
No. 2	4	0.2	< 0.1	Pitted surface
LEAD WRAPPED MODELS				
No. 1	5	9.0	31.5	
No. 2	7	13.5	50.0	
FLOW REGION MODELS				
Helical No. 1	8	0.1	< 0.1	Pitted surface
Helical No. 2	9	0.5	< 0.3	Small crater, off axis
Ring No. 1	10	0.2	0	
Ring No. 2	11	0.1	0	Slightly pitted
FLOW REGION MODELS WITH EXPANSION CHAMBER				
Helical No. 1	15	3.8	5.8	
Helical No. 2	16	6.5	15.2	
Ring No. 1	13	2.7	5.0	
Ring No. 2	14	3.8	7.5	
ENHANCED JETTING				
H.E. Products--Standard	20	7.0	15.5	
H.E. Products--Steel Helix	21	0.1	< 0.1	Slightly pitted surface
Collapsed Pipe--Standard	2E	12.6	13.8	
Collapsed Pipe--Steel Helix	22E	0.4	< 0.3	Off-axis crater
1 ATMOSPHERE				
Standard	17	6.5	24.5	
Steel Helix	19	< 0.2	< 0.1	
SOURCE CHARACTERIZATION				
30 cm Helix/100 cm Tube	22	5.0	9.4	Irregular off-axis crater
30 cm Helix/65 cm Tube	4E	Not Recovered		
30 cm Helix/30 cm Tube	6E	Not Recovered		
30 cm Helix/30 cm Tube Expansion Chamber	18E	Not Recovered		
50 cm Stand-Off	20E	1.3 (Ring)	2.3	Ring crater
90° Bend in Pipe	23	Not Recovered		

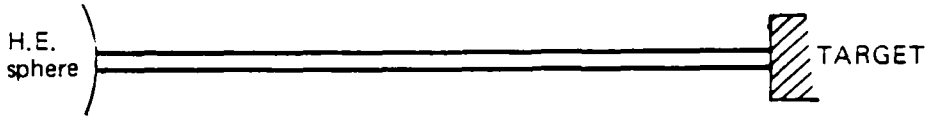

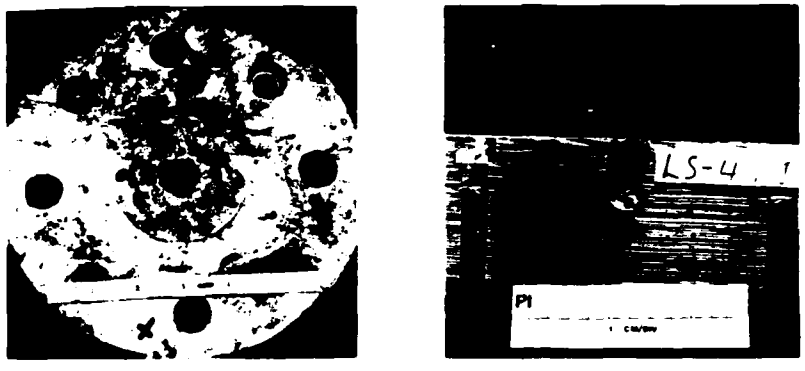

DEPTH = 4.1 cm
VOLUME = 14.8 cm^3

MODEL 1 (Standard No. 1)

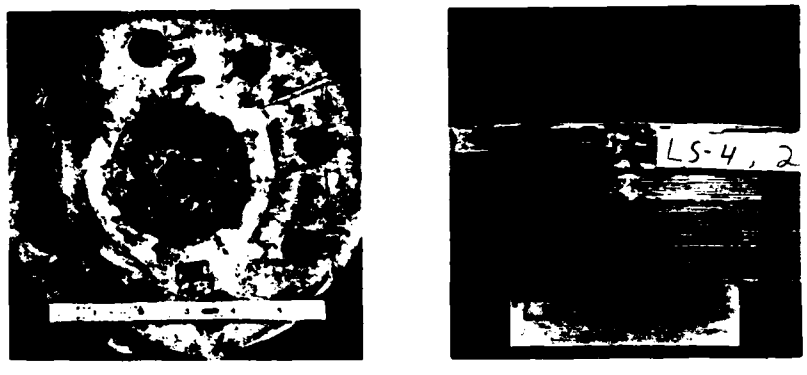

DEPTH = 4.0 cm
VOLUME = 9.0 cm^3

MODEL 2 (Standard No. 2)

Figure 20 Comparison of target damage from the two standard Models 1 and 2

internal helix eliminated or significantly reduced target damage, as is shown in Figure 21. The depths and volumes were very small, generally less than 0.1 cm or 0.1 cm^3. There are some small pockmarks on the surface, but it is not possible to determine if these were caused by the primary penetrating jet or by secondary ejecta.

3.7.3 Effect of Air Within the Model (Models 17 and 19). Model 17 was similar in construction to Models 1 and 2 but was not evacuated. The results of this model showed a depth and volume similar to those obtained for the standard evacuated models, thus suggesting that one atmosphere of air does not significantly alter the jet forming process.

Similar conclusions were reached for Model 19, which was constructed similar to Models 3 and 4, which contained helices; but this model, like Model 17, contained one atmosphere of air. The result was that no penetrating jet reached the target. Photographs of these two targets are shown in Figure 22.

3.7.4 Effects of LOS Tube Areal Density (Models 5 and 7). For these models, a thick lead tube was slid over the normal LOS pipe, increasing the areal density of the LOS tube by a factor of 10. The penetration depths of 9.0 and 13.5 cm were some of the deepest recorded and very similar to that recorded for a similar model, Model 8 in the LS-2 experiment, with a depth of 9.2 cm. The target photographs are shown in Figure 23. There is an enlargement of the crater about 2-1/2 cm from the face of the target for Model 7, which corresponds to the section plane that contained the carbon stress gage. This enlargement suggests that

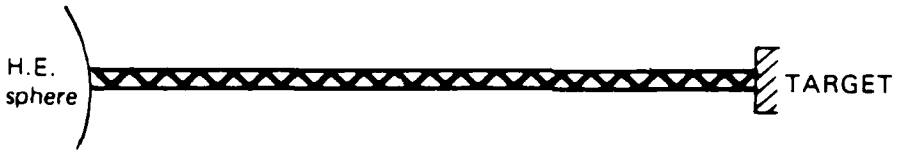

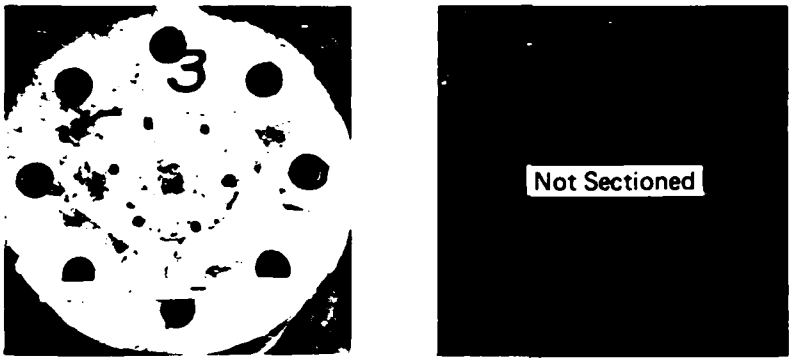

DEPTH = < 0.1 cm
VOLUME = < 0.1 cm^3

MODEL 3 (Helix 1)

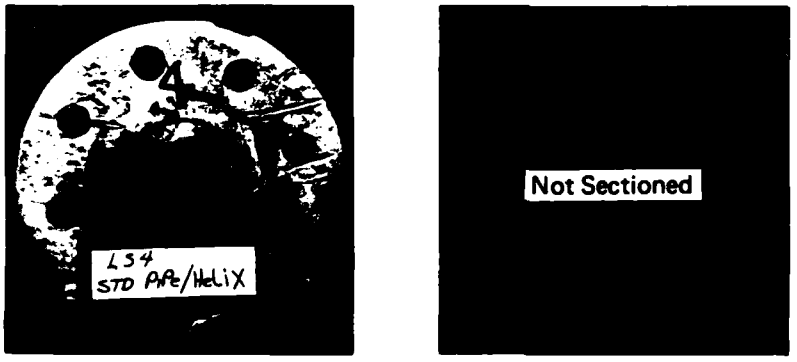

DEPTH = 0.2 cm
VOLUME = < 0.1 cm^3

MODEL 4 (Helix 2)

Figure 21 Comparison of target damage from the two LOS pipe models containing steel helixes (Models 3 and 4)

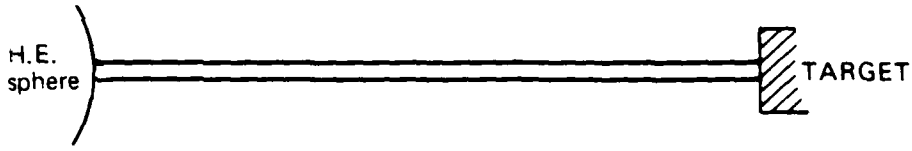

DEPTH = 6.5 cm

VOLUME = 24.5 cm^3

MODEL 17 (Standard LOS – Atmospheric)

DEPTH = < 0.2 cm

VOLUME = < 0.1 cm^3

MODEL 19 (Helix – Atmospheric)

Figure 22 Comparison of targets from models containing one atmosphere of air, Model 17 without a helix and Model 19 with a helix

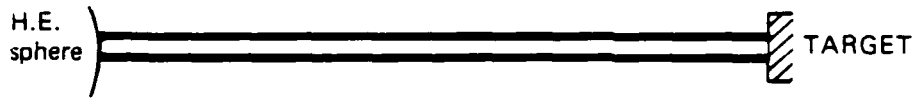

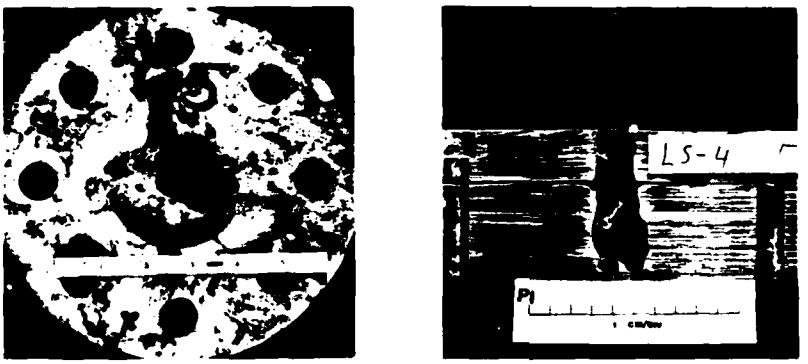

DEPTH = 9.0 cm
VOLUME = 31.5 cm^3

MODEL 5 (Lead Wrap No. 1)

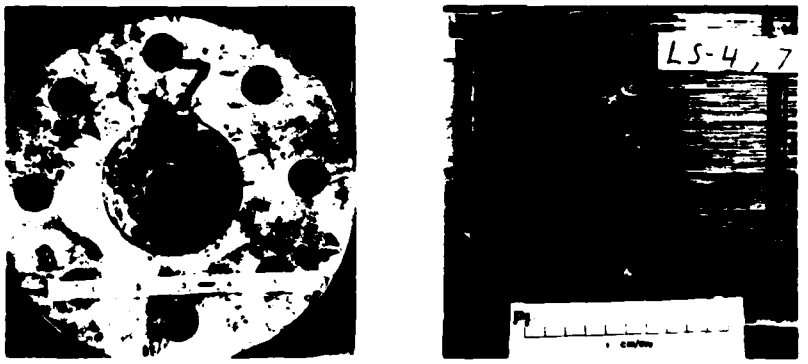

DEPTH = 13.5 cm
VOLUME = 50.0 cm^3

MODEL 7 (Lead Wrap No. 2)

Figure 23 Target photographs from Models 5 and 7, which had an additional 2 mm lead tube placed over the standard LOS pipe

the target plates probably separated slightly during the time of jet penetration. Again, these data suggest that the areal density of the LOS pipe plays an important role in the amount of penetration observed.

3.7.5 Explosive Product Models (Models 20 and 21). These two models were fabricated to allow nitromethane from the sphere to enter the tube for a distance of 38 mm. One model used a standard tube and the other used a helix to determine if the jet would be enhanced and, if so, if the helix would still eliminate it. The target penetration of 7.0 cm, with a volume of 15.5 cm^2, was slightly larger than the mean penetration of standard models. The volume was slightly lower than mean. Target photographs are shown in Figure 24. Model 21 with the helix was again totally effective in defeating the jet. Only small, minor surface impacts were observed.

3.7.6 High Explosive Precollapsed Pipes (Models 2E and 22E). For these models, the pipe extended 216 mm into the sphere containing high explosives to determine if this configuration would enhance the jet during the early collapse and jet formation. One model used a standard LOS pipe, while the other included a helix to determine its effectiveness. The results are shown in Figure 25.

The penetration depth of 12.6 cm and volume of 43.8 cm^3 for Model 2E without a helix did show values larger than normal for standard model targets. The helix was quite effective in defeating the jet. The target showed only 0.4 cm of maximum

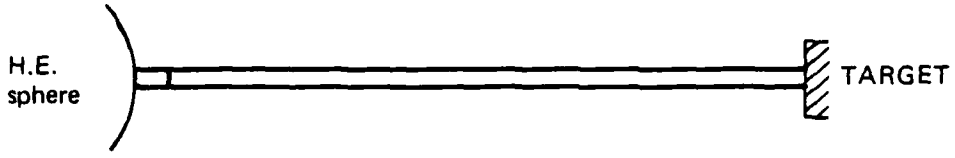

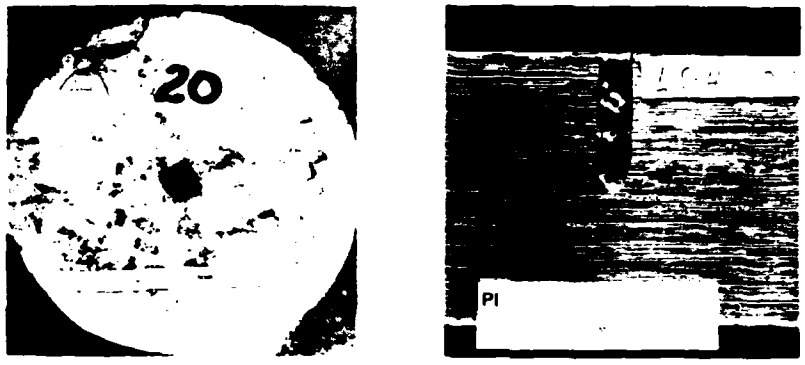

DEPTH = 7.0 cm
VOLUME = 15.5 cm^3

MODEL 20 (Explosive Products)

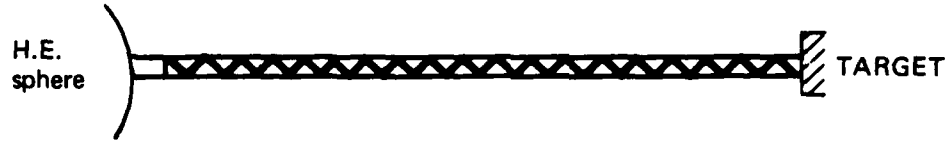

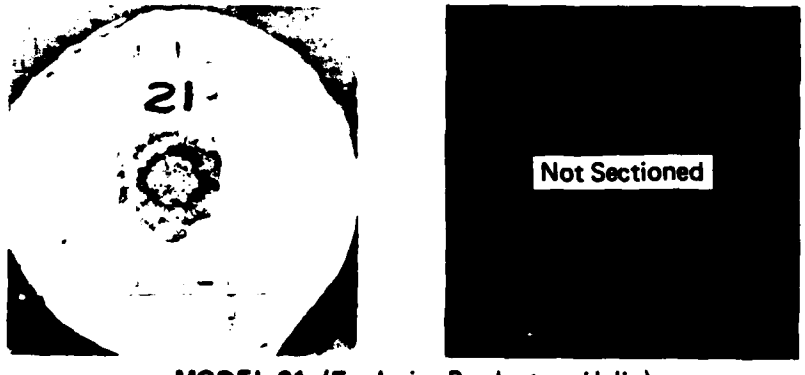

DEPTH = 0.1 cm
VOLUME ≈ < 0.1 cm^3

MODEL 21 (Explosive Products – Helix)

Figure 24 Comparison of target damage from models with and without a helix which had nitromethane in the first 38 mm of the pipe (Models 20 and 21 of LS-4)

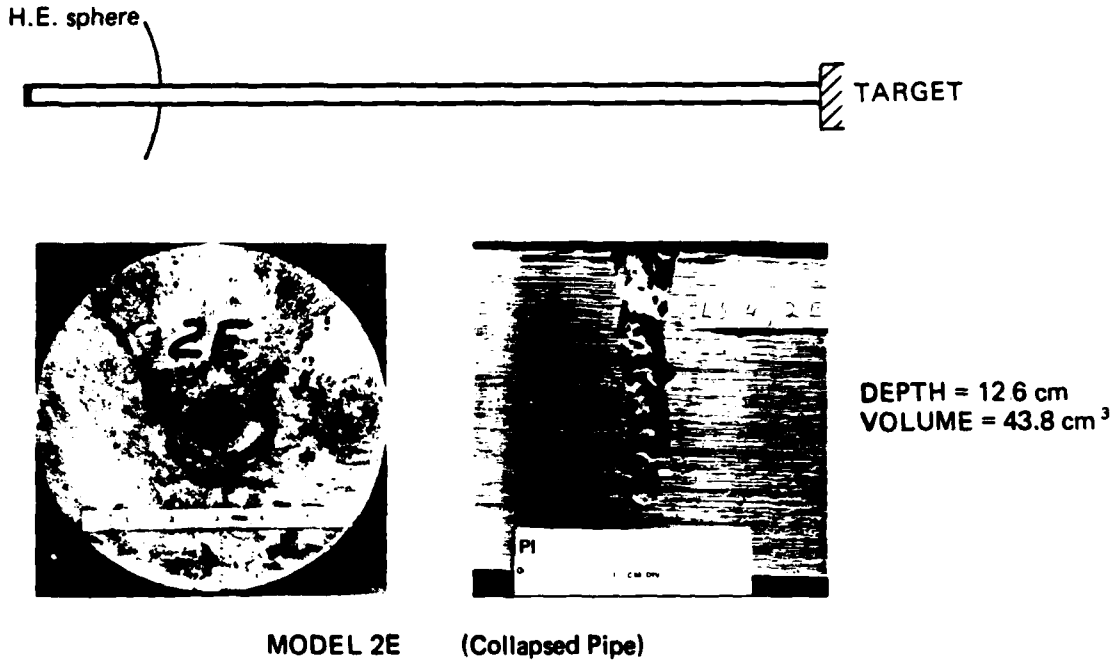

Figure 25 Comparison of target damage from models with and without a helix when the LOS pipe extended 216 mm into the sphere containing high explosives (Model 2E and 22E of LS-4)

penetration depth and less than 0.3 cm^3 of volume, which is very close to totally defeating the jet.

3.7.7 Pipe Standoff (Model 20E). To further evaluate the length of LOS pipe that contributes to producing the jet, the LOS pipe of Model 20E was plugged with a 500-mm rod of plastic. This effectively shortened the length of the LOS pipe and provided a standoff of this distance. The results shown in Figure 26 dramatically demonstrate that the target damage is reduced to a penetration depth of only 1.3 cm with a volume of 2.3 cm^3. In addition, the crater is ring-like, with its outer diameter about the same as the original pipe diameter. This observation suggests that the penetrating jet in this case did not travel on the pipe axis but flowed along the LOS pipe wall. There were a number of models fielded on previous tests with different standoff lengths (or plugs), and the penetration volume data from these tests are shown in Figure 27 along with the LS-4 datum. The data suggest a much better fit than might be expected considering the data scatter that has been observed for eight identical standard models. The data trend, however, should be valid and the scatter should diminish as the volumes approach zero. The data suggest that jet formation occurs in the first 55 to 60 cm of standard LOS pipe length.

3.7.8 Source Region Jet Characteristics (Model 22). Three model configurations were used to evaluate whether a short 32-cm helix placed in the source region would defeat the jet and whether the target penetration would vary as the target was placed nearer to the source regions. Unfortunately, only the target from Model 22 with the target placed at the standard

DEPTH = 5.0 cm
VOLUME = 9.4 cm^3

MODEL 22

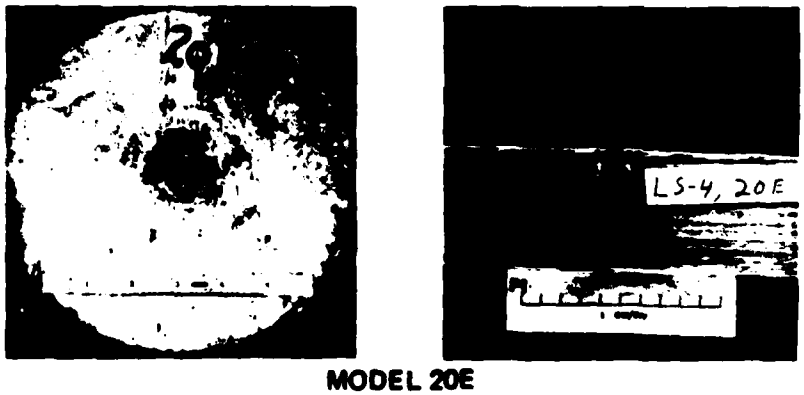

DEPTH = 1.3 cm
VOLUME = 2.3 cm^3

MODEL 20E

Figure 26 Photograph of target damage from Model 20E (50 cm standoff) and Model 22 (source region steel helix)

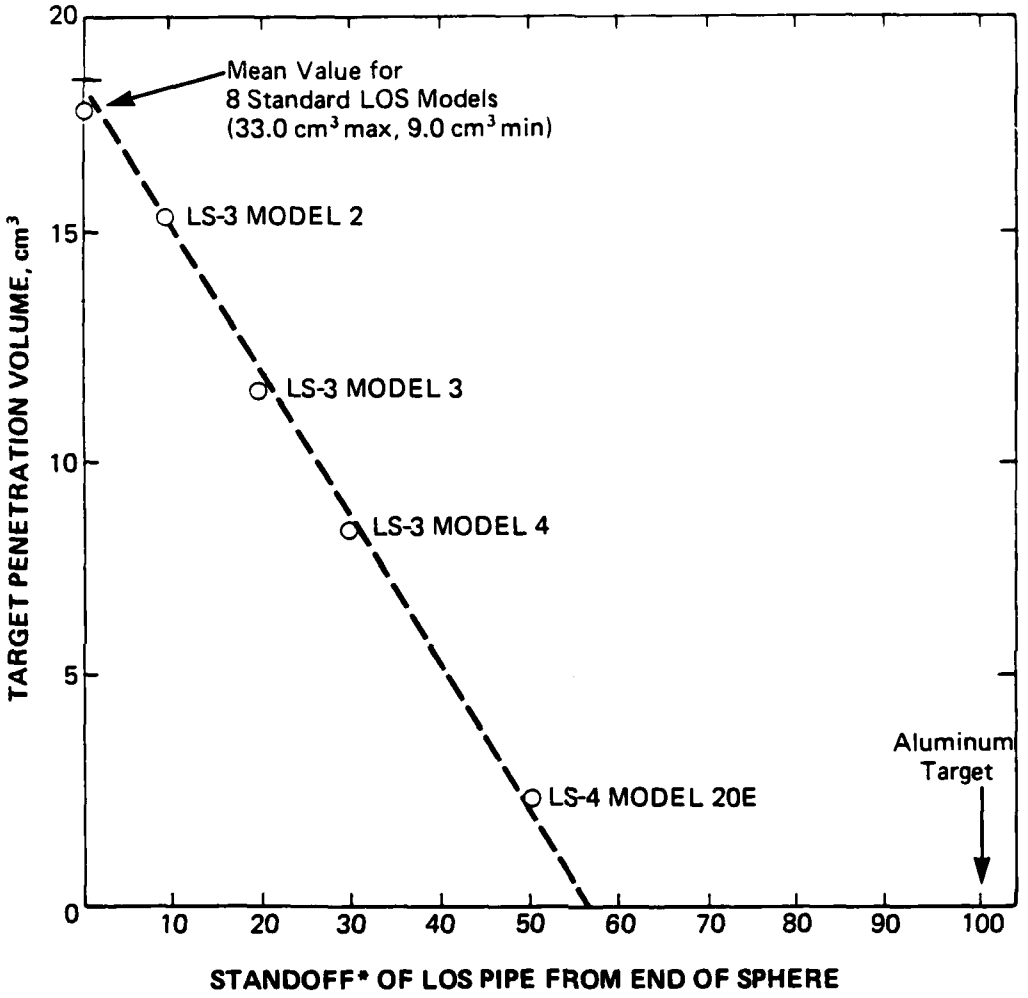

82-2-101

(*NOTE – A standard length pipe was used and a plug was inserted to change the standoff distance)

Figure 27 Plot of all LOS target penetration volume data as a function of LOS pipe standoff from the high explosive sphere

distance was recovered. This target, shown in Figure 26, has a very non-axial penetration with a total depth of 5.0 cm and a penetration volume of 9.4 cm^3. If one assumes the helix is effective in the source region in defeating the jet, then it should act similar to a plug in an LOS pipe. Using this assumption and plotting the penetration volume value on Figure 27, the data point is found to fall very close to the line of that graph.

The penetration volume was surprising, however, since it is in contradiction to the data from two models in the LS-3 experiment in which a polyolefin helix of different lengths was used in the source region. In that experiment, Model 15 used a 15.2-cm-long helix which produced a 12.2 cm^3-deep crater while a 22.9-cm-long polyolefin helix used on Model 16 produced a 2.8-cm^3 crater. For convenience these data are plotted in Figure 28, which includes the data fit of pipe standoff from Figure 27. The data from Model 16 of LS-3 would be significantly off the data line. This deviation suggests, among a number of possibilities, that either the data scatter from all these tests is too large to use in this detailed an examination or that polyolefin helices are more effective than steel in defeating jets.

3.7.9 Flow Region Asymmetries (Models 8, 9, 10, and 11). To assess the effectiveness of helices placed outside the collapse region of the LOS pipe, four models were used where the asymmetry was located only 384 mm from the target, well outside the region of jet generation as shown in Figure 28. Two models, numbers 8 and 9, used standard helical asymmetries while in Models 10 and 11 ring asymmetries were used (see Figure 5 for a description of helical and ring asymmetries).

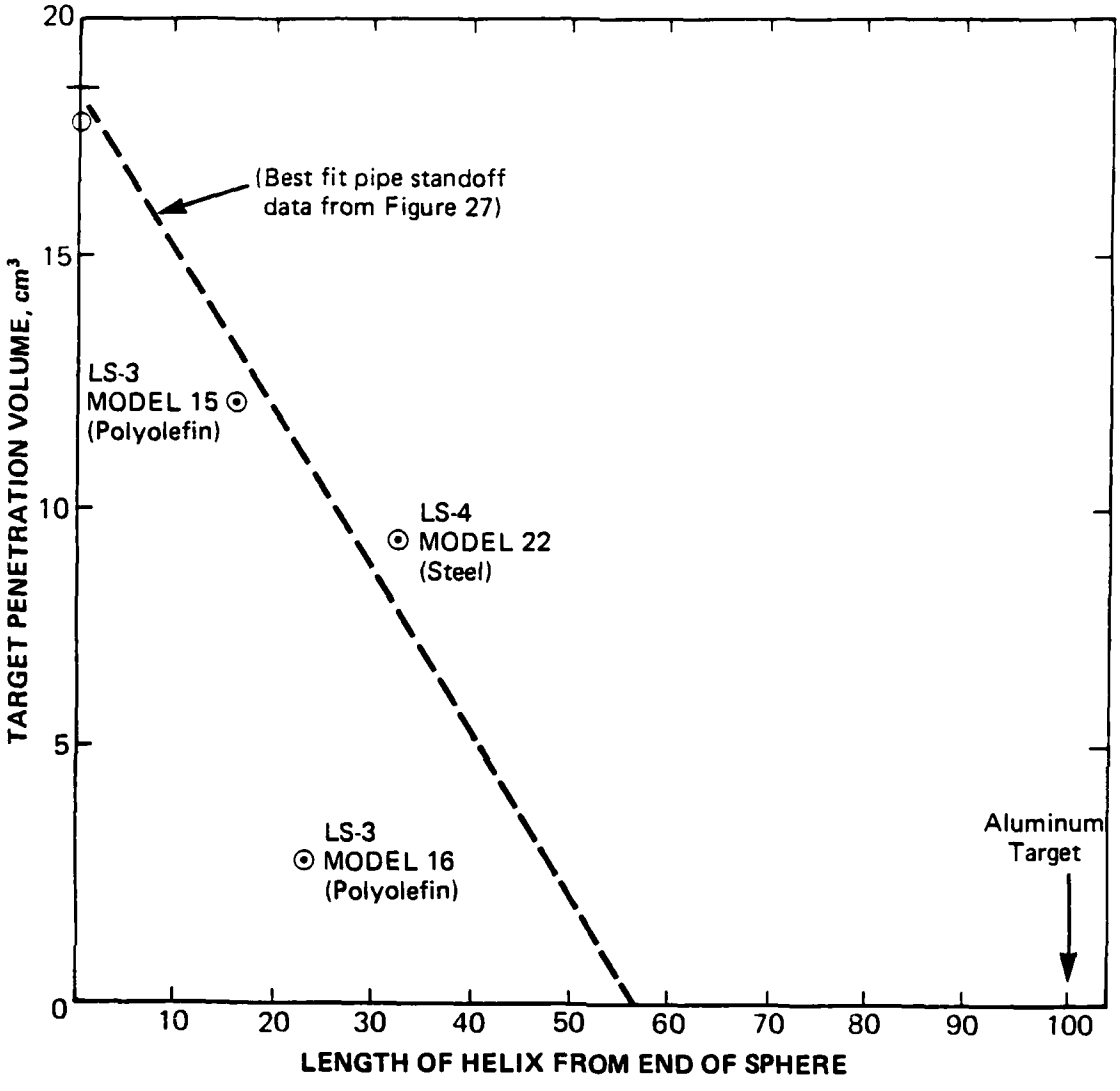

82-3-136

Figure 28 Plot of all LOS target penetration volume data as a function of length of helix from the high explosive sphere

The results were quite similar to those observed for Model 12 in the LS-3 experiment where a thick lead helix effectively defeated the jet. Figure 29 photographically shows the target damage from these models. These short helical asymmetries were almost as effective as a full length helix, with a maximum depth of 0.5 cm and volume of less than 0.3 cm^3 measured for the target on Model 9.

The models containing ring asymmetries were also quite effective, with a maximum penetration of 0.2 cm and a nonmeasurable volume recorded for Model 10.

From these data it appears that the helix is just as effective in defeating the jet if it is placed outside the jet-forming region and that no significant improvement is gained in using a full length helix. The conclusion we reach is that the helix operates by attenuating the jet flow, not by altering jet formation.

3.7.10 Flow Region Asymmetries Placed in an Expansion Chamber (Models 13, 14, 15, and 16). In these tests an expansion chamber was placed in the flow region and thick helices and rings were inserted inside the expansion chamber so that their inside surfaces were just flush with the inside diameter of the standard LOS pipe. The expansion chamber, which is somewhat analogous to the muffler designs on UGT events, was used to determine if its use would be beneficial.

The helical models were numbers 15 and 16, and the target damage from these models is shown in Figure 30. As can be seen,

MODEL 8

MODEL 9

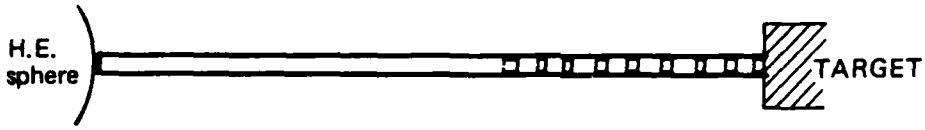

MODEL 10

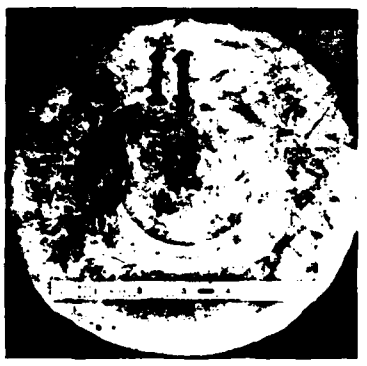

MODEL 11

Figure 29 Target damage from models containing helical asymmetries (Models 8 and 9) and ring asymmetries (Models 10 and 11) located only in the flow region of the LOS pipe

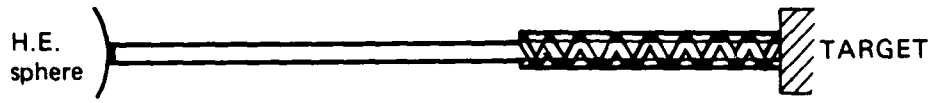

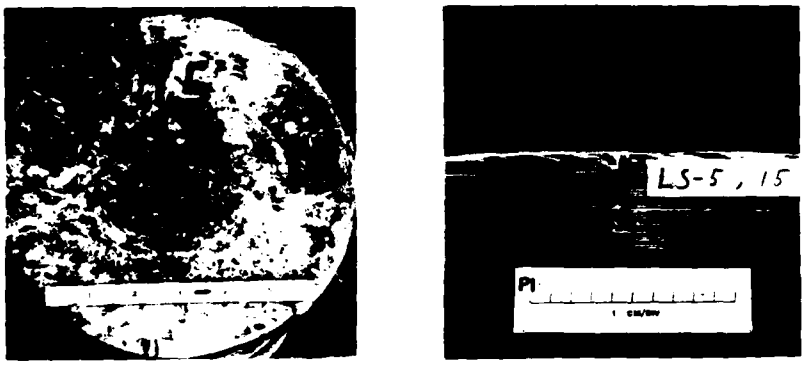

DEPTH = 3.8 cm
VOLUME = 5.8 cm^3

MODEL 15 (Helix No. 1)

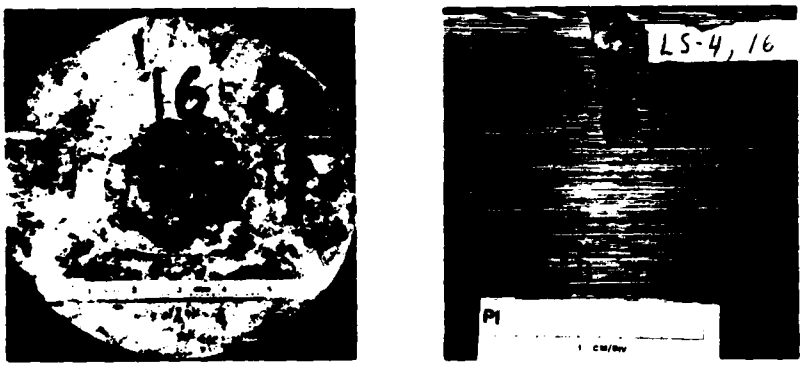

DEPTH = 6.5 cm
VOLUME = 15.2 cm^3

MODEL 16 (Helix No. 2)

Figure 30 Target damage from models 15 and 16 that used an expansion chamber (larger diameter pipe) in the flow region of the LOS pipe in which helical assymetries were placed flush with the ID of the LOS pipe

significant damage occurred, with Model 16 producing a 6.5-cm-deep hole with a volume of 15.2 cm^3, well within the standard deviation of the standard LOS target damage data.

Likewise, the ring asymmetry models also produced large target damage with a 3.8-cm-deep, 7.5-cm^3-volume crater in the target of Model 14 shown in Figure 31.

The only significant difference between these models and those previously described (without an expansion chamber) was that (1) these asymmetries were solidly attached to the expansion chamber walls and (2) they did not protrude below the inside surface of the LOS pipe.

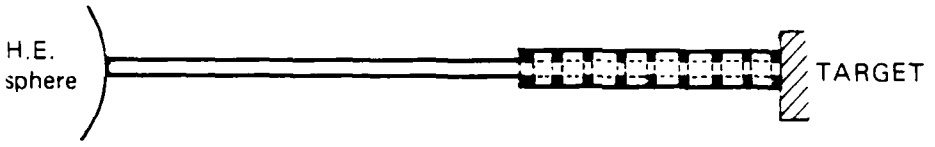

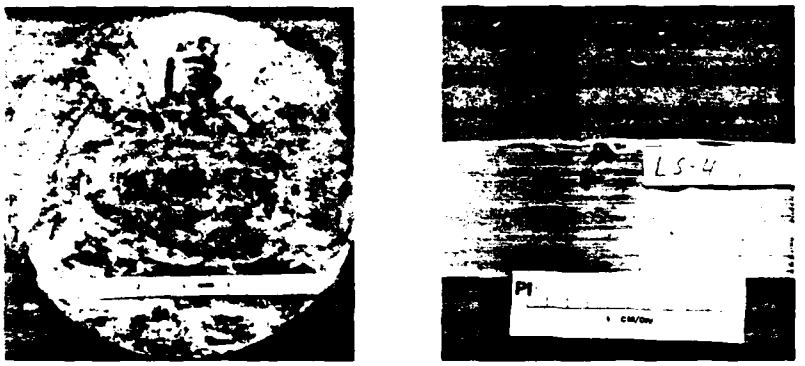

DEPTH = 2.7 cm
VOLUME = 5.0 cm^3

MODEL 13 (Ring No. 1)

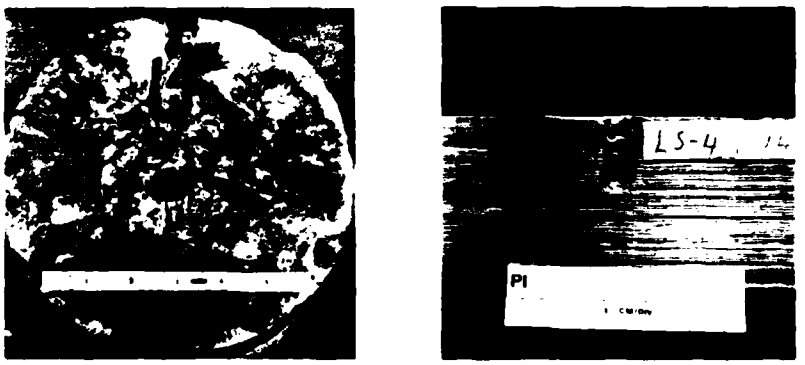

DEPTH = 3.8 cm
VOLUME = 7.5 cm^3

MODEL 14 (Ring No. 2)

Figure 31 Target damage from models 13 and 14 that used an expansion chamber (larger diameter pipe) in the flow region of the LOS pipe in which ring asymmetries were placed flush with the ID of the LOS pipe.

SECTION 4

SUMMARY OF EXPERIMENT RESULTS

The major findings of the LS-4 experiment were:

- Two standard evacuated LOS pipe models produced high-energy jets that caused deep craters in aluminum targets located at the end of the models. The penetration depth was reproducible; the volume was not. When these data are added to the LS-2 and LS-3 data base, the mean crater depth of the eight targets becomes 17.8 cm^3 with a standard deviation of 8.4 cm^3.

- The use of air instead of the normal few microns of vacuum in the pipe model did not affect the jet within the limits of the data scatter.

- A 2-mm-thick lead sleeve placed over two standard pipe models produced penetration craters significantly larger than those produced by the standard LOS pipe models.

- When the end of a standard model was extended into the nitromethane sphere, a larger than average target penetration depth volume was produced.

- Allowing the liquid explosive to extend into the LOS pipe model produced a jet whose penetration was very similar to those of the standard model.

- For all the above LOS pipe models, loosely attached internal steel helices were extremely effective in eliminating target damage. In all cases, the maximum crater depths were less than 0.2 cm, and volumes were less than 0.3 cm^3.

- Data from standard models with standoffs on this experiment combined with similar data from previous experiments indicates that the region of jet formation probably does not extend beyond 60 cm from the surface of the nitromethane sphere for standard models.

- Helical and ring asymmetries were also effective in eliminating target damage even when the asymmetry was relatively short and was located only near the target, well beyond the region where jet formation occurs. This indicates that the helix operates by attenuating the jet flow.

- When the helical and ring asymmetries just described were inserted into larger diameter expansion chambers such that the inner surface of the asymmetry was flush with the inside diameter of the standard model pipe, little or no attenuation of the jet was observed.

In addition to the findings given above, results were obtained from the active instrumentation placed on selected models and targets. Ionization switches placed through the wall of the models showed initial jet velocities from 0.84 to 1.2 cm/μs. In general, these data are consistent with data from previous experiments, although the 1.2 cm/μs velocity calculated for the standard model was higher than expected.

Penetration pins and stress gages located in the targets confirmed that the initial high velocity jet is probably gaseous and does not contain sufficient energy to penetrate the target or cause any measurable internal stress in the target. The penetrating jet velocities in the LOS pipes, measured from the time of initial pressure arrival, were 0.53 cm/μs for the lead wrapped model and 0.59 cm/μs for the standard model. The data from the two lead-wrapped-model targets with 9.0 and 13.5 cm of penetration showed very linear penetration rates in the aluminum targets

of 0.058 and 0.062 cm/μs, respectively, for 5 cm of penetration depth. The stress gages located inside the target showed that the stress increases as the penetrating jet approaches; and the gage is destroyed as it is penetrated. Unfortunately, the pressure gages monitoring the pressure in the model at a location just in front of the target did not yield meaningful data.

REFERENCES

1. E. T. Moore, Jr. and R. Funston, "Asymmetric Collapse of LOS Pipe," DNA Report DNA 5023F, July 1979.

2. E. T. Moore, Jr. and R. Funston, "Asymmetric Collapse of LOS Pipe," DNA Report DNA 5322F, May 1980.

DISTRIBUTION LIST

DEPARTMENT OF DEFENSE

Defense Nuclear Agency
ATTN: SPTD, T. Kennedy
4 cy ATTN: TITL

Defense Technical Information Center
12 cy ATTN: DD

Field Command
Defense Nuclear Agency
ATTN: FCTT, G. Ganong
ATTN: FCTT, W. Summa
ATTN: FCT, COL G. Ballantine
3 cy ATTN: FCTK, B. Ristvet
3 cy ATTN: FCTK, C. Keller

DEPARTMENT OF ENERGY

Department of Energy
Nevada Operations Office
ATTN: R. Newman

OTHER GOVERNMENT AGENCY

Department of the Interior
US Geological Survey
ATTN: R. Carroll
ATTN: A. Fernald

DEPARTMENT OF ENERGY CONTRACTORS

Desert Research Institute
ATTN: D. Schulke Sec Off for P. Fenske
ATTN: D. Schulke Sec Off for C. Case

University of California
Lawrence Livermore National Lab
ATTN: B. Hudson
ATTN: F. Morrison
ATTN: L-209, G. Higgins
ATTN: R. Terhune
ATTN: L. Makague

DEPARTMENT OF ENERGY CONTRACTORS (Continued)

Los Alamos National Laboratory
ATTN: T. Kunkle, ESS-5
ATTN: R. Brownlee
ATTN: C. Keller
ATTN: F. App
ATTN: B. Travis

Sandia National Lab
ATTN: C. Smith
ATTN: Org 7112, C. Mehl

DEPARTMENT OF DEFENSE CONTRACTORS

California Research & Technology, Inc
ATTN: M. Rosenblatt

Kaman Tempo
ATTN: DASIAC

Pacific-Sierra Research Corp
ATTN: H. Brode, Chairman SAGE

Pacifica Technology
ATTN: D. Patch

Physics International Co
4 cy ATTN: E. Moore, Jr
4 cy ATTN: D. Mumma
4 cy ATTN: J. Thomsen
4 cy ATTN: F. Funston

R&D Associates
ATTN: P. Haas

S-CUBED
ATTN: R. Duff
ATTN: C. Dismukes

SRI International
ATTN: A. Florence


DATE
ILME